Comput. Methods Appl. Mech. Engrg. 198 (2009) 2768–2784

Contents lists available at ScienceDirect

Comput. Methods Appl. Mech. Engrg.

journal homepage: www.elsevier.com/locate/cma

Robin–Robin preconditioned Krylov methods for fluid–structure interaction problems ☆

Santiago Badia [a], Fabio Nobile [b], Christian Vergara [c,*]

[a] International Center for Numerical Methods in Engineering (CIMNE), Universitat Politècnica de Catalunya, Jordi Girona 1-3, Edifici C1, 08034 Barcelona, Spain
[b] MOX, Dipartimento di Matematica, Politecnico di Milano, Piazza L. Da Vinci 32, 20133 Milano, Italy
[c] Dept. of Information Technology and Mathematical Methods, Università degli Studi di Bergamo, Viale Marconi 5, 24044 Dalmine (BG), Italy

ARTICLE INFO

Article history:
Received 14 August 2008
Received in revised form 30 March 2009
Accepted 5 April 2009
Available online 22 April 2009

MSC:
65M12
65M60

Keywords:
Fluid–structure interaction
Partitioned procedures
Domain decomposition preconditioners
Robin boundary conditions
Added-mass effect
Hemodynamics
Enclosed fluid problems

ABSTRACT

In this work, we propose a Robin–Robin preconditioner combined with Krylov iterations for the solution of the interface system arising in fluid–structure interaction (FSI) problems. It can be seen as a partitioned FSI procedure and in this respect it generalizes the ideas introduced in [S. Badia, F. Nobile, C. Vergara, J. Comput. Phys. 227 (2008) 7027–7051]. We analyze the convergence of GMRES iterations with the Robin–Robin preconditioner on a model problem and compare its efficiency with some existing algorithms. The method is shown to be very efficient for many challenging fluid–structure interaction problems, such as those characterized by a large added-mass effect or by enclosed fluids. In particular, the possibility to solve balloon-type problems without any special treatment makes this algorithm very appealing compared to the computationally intensive existing approaches.

1. Introduction

In this paper, we focus on the solution of the time-dependent fluid–structure interaction (FSI) problem, which arises when an incompressible fluid interacts with a structure. In particular, we focus on *modular* algorithms that allow to reuse pre-existing fluid and structure codes.

We are interested in those FSI problems where the *added-mass effect* is high, that is when the ratio between the fluid and structure densities is close to one (or larger). This typically appears in hemodynamic applications. It has been reported in the literature [41,9,18,29] that the solution of the FSI system using explicit partitioned approaches (also called loosely coupled) is problematic in this situation. We refer to [44] for a discussion about the added-mass effect for compressible flows. In general, explicit algorithms that solve only once (or just few times) per time step the fluid and structure sub-problems are unstable, unlike for low added-mass problems such as those arising in aeroelasticity.

To obtain stable numerical schemes to solve the monolithic system, one has then to consider algorithms that enforce exactly at each time step the continuity of the velocity and normal stresses at the fluid–structure interface. Among them, we consider modular algorithms that involve separate fluid and structure evaluations and that interact through the exchange of suitable transmission conditions on the interface. These algorithms are based on domain decomposition preconditioners (see [11]), which are applied to the *interface equation* (Schur complement) related to the whole FSI system. Then, the preconditioned system is solved using an iterative solver. Let us note that any approach employing domain decomposition preconditioners is monolithic, in the sense that it provides the monolithic solution. Thus, at convergence, they guarantee the continuity of the velocity and the normal stress at the interface (strong coupling).

These preconditioned systems are usually solved with (relaxed) Richardson iterations as iterative solver. The most popular of such schemes is the so-called *Dirichlet–Neumann* (DN) algorithm, which consists in solving iteratively the fluid equations, given the structure velocity at the FSI interface (Dirichlet boundary condition), and the

☆ S. Badia's research was supported by the European Community through the Marie Curie contract *NanoSim* (MOIF-CT-2006-039522). The research of F. Nobile and C. Vergara has been partially supported by the Italian grant PRIN 2007 'Numerical modelling for scientific Computing and advanced applications'.

* Corresponding author.
E-mail addresses: sbadia@cimne.upc.edu (S. Badia), fabio.nobile@polimi.it (F. Nobile), christian.vergara@unibg.it (C. Vergara).

0045-7825/$ - see front matter © 2009 Elsevier B.V. All rights reserved.
doi:10.1016/j.cma.2009.04.004

structure equations, given the fluid normal stress at the interface (Neumann boundary condition). However, it has been shown in [9] that in presence of a large added-mass effect, the DN procedure needs a strong relaxation and features a very slow convergence. In [11], Neumann–Dirichlet and Neumann–Neumann preconditioners (see [37]) have been applied with Richardson iterations. In [2] a new class of iterative procedures based on Robin transmission conditions has been introduced (*Robin–Robin (RR) schemes*), which generalizes the Dirichlet–Neumann approach. In particular, the results in [2] indicate that among all possibilities, the *Robin–Neumann* (RN) algorithm exhibits very good performances for a wide range of added-mass and is by far more efficient than the DN strategy. More recently, in [5] RR schemes have been extended to a fluid coupled with a poroelastic incompressible structure.

On the same lines, [27] and more recently [3] propose preconditioned Krylov iterations over the interface equation, instead of Richardson iterations. In particular, [27] considers preconditioned Newton–Krylov methods, whereas [3] analyzes both theoretically and numerically the DN preconditioned GMRES method applied to a suitable linearization of the interface equation. The results in [3] have highlighted the better performance of DN-GMRES compared to the DN-Richardson version, in presence of a large added-mass effect.

For completeness, we also mention other monolithic approaches that have been recently proposed, which however are not modular and do not lead to separate solutions of fluid and structure subsystems. Again, the efficiency of non-modular approaches will depend on how good (and cheap) is the preconditioning. Among these, we mention the strategies based on the application of GMRES to the monolithic system [23,16]. Realistic vascular problems have been solved in [6,7] using a diagonal preconditioner and GMRES iterations over the whole FSI system (see also [42,43]). In [3], more elaborated non-modular ILUT preconditioners and Schur complement preconditioners (called PIC schemes) have been compared in terms of computational cost for test problems with large added-mass effect. In [14], the authors propose a particular coupled FSI problem where the well-known Chorin–Temam method is used for the fluid subsystem. The pressure Poisson equation is kept strongly coupled to the structural problem to obtain a stable discretization. Similar ideas, but on a purely algebraic level, have been investigated in [33,4] where the algebraic Chorin–Temam scheme (see [31]) and the Yosida scheme (see [35,34]), have been extended to the FSI problem. Finally, we mention the work [8] which proposes a global weak formulation relying on the imposition of the kinematic coupling conditions (continuity of the velocity at the interface) by the Nitsche method.

The goal of the present work is two-fold. Firstly, moving from the idea proposed in [27,3], we reinterpret the Robin–Robin partitioned scheme introduced in [2] as a preconditioned Richardson algorithm (RR-Richardson) over the Schur complement equation, and identify the corresponding preconditioner. This allows us to further apply the RR-preconditioner together with more efficient Krylov methods such as GMRES (RR-GMRES). In particular, we focus on the Robin–Neumann GMRES method (RN-GMRES) and provide a theoretical convergence analysis for a model linear FSI problem as well as a numerical comparison of performances among RN-Richardson, RN-GMRES and DN-GMRES.

We also study the sensitivity of RN-Richardson and RN-GMRES with respect to the coefficient appearing in the Robin transmission condition. A good candidate for such coefficient has been given in [30] in the context of hemodynamics applications.

The second goal of this paper is to propose the algorithms based on the RN preconditioner as effective tools to solve enclosed fluid problems, where only Dirichlet or flow rate boundary conditions are prescribed on the fluid boundary (excluding the FS interface). It is well known that this kind of problems cannot be solved with a straightforward application of the DN technique, since the mass conservation law is in general violated [22,29], and specific treatments, such as the introduction of Lagrange multipliers or artificial compressibility, must be considered (see Section 7.1).

In both cases, the computational costs are quite high. On the contrary, our Robin condition-based algorithms can be straightforwardly applied to this kind of problems. Let us note that non-modular preconditioners have no difficulty solving fluid–structure interaction problems in fully enclosed domains (see [7,42]).

The outline of the paper is as follows. In Section 2 we set the FSI problem both in its continuous and time-discrete forms and derive the algebraic interface problem. In Section 3, we reinterpret the RR partitioned procedure proposed in [2] as partitioned Richardson iterations on the algebraic interface problem and identify the corresponding preconditioner. In Section 4, we analyze the RR-GMRES solver and reducing it to a sequence of calls to fluid and structure solvers with suitable Robin boundary conditions, whilst in Section 5 we highlight its modularity. In Section 6, we provide the convergence analysis of the RN-GMRES scheme applied to a model linear FSI problem. In Section 7, we review the difficulties related to the solution of enclosed flow problems by traditional partitioned procedures (such as DN) and show how RR-preconditioned Krylov methods naturally overcome such difficulties In Section 8, we present several 2D and 3D numerical results, confirming the theoretical observations of the previous sections and finally in Section 9 we draw some conclusions.

2. Problem setting

2.1. The continuous FSI problem

Let us consider the fluid–structure domain $\Omega^t \subset \mathbb{R}^d$ ($d = 2, 3$, being the space dimension), where t here denotes time. This domain is divided into a sub-domain Ω_s^t occupied by an elastic structure and its complement Ω_f^t occupied by the fluid (see Fig. 1). The fluid–structure interface Σ^t is the common boundary between Ω_s^t and Ω_f^t, i.e. $\Sigma^t = \partial\Omega_s^t \cap \partial\Omega_f^t$. Furthermore, $\boldsymbol{n}_f$ is the outward normal to Ω_f^t on Σ^t and $\boldsymbol{n}_s = -\boldsymbol{n}_f$ is its counterpart for the structure domain. The initial configuration Ω^0 at $t = 0$ is considered as the reference one. In order to describe the evolution of the whole domain Ω^t we define two families of mappings:

$$\mathscr{L} : \Omega_s^0 \times (0,T) \to \Omega_s^t, \quad (\boldsymbol{x}_0, t) \mapsto \boldsymbol{x} = \mathscr{L}(\boldsymbol{x}_0, t)$$

and

$$\mathscr{A} : \Omega_f^0 \times (0,T) \to \Omega_f^t, \quad (\boldsymbol{x}_0, t) \mapsto \boldsymbol{x} = \mathscr{A}(\boldsymbol{x}_0, t).$$

The maps $\mathscr{L}^t = \mathscr{L}(\cdot, t)$ and $\mathscr{A}^t = \mathscr{A}(\cdot, t)$ track the solid and the fluid domains in time. Due to the continuity of the velocity at the interface, the two mappings have to satisfy the condition

$$\mathscr{L}^t = \mathscr{A}^t \quad \text{on } \Sigma^t, \quad \forall t \in (0,T). \tag{1}$$

To describe the structure kinematics we use a Lagrangian framework. Therefore, the solid mapping $\mathscr{L}^t$ is straightforwardly determined by

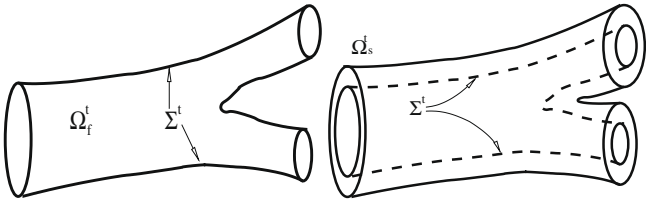

Fig. 1. Example of domain Ω^t. Fluid domain Ω_f^t (left) and solid domain Ω_s^t (right).

$$\mathscr{L}^t(\boldsymbol{x}_0) = \boldsymbol{x}_0 + \hat{\boldsymbol{\eta}}(\boldsymbol{x}_0, t),$$

where $\hat{\boldsymbol{\eta}}$ denotes the displacement of the solid medium with respect to the reference configuration.

The fluid problem is stated in an *Arbitrary Lagrangian–Eulerian* (ALE) framework (see e.g. [24,13]). The fluid domain mapping $\mathscr{A}^t$ is defined by an arbitrary extension of its value on the interface, which is given by condition (1):

$$\mathscr{A}^t(\boldsymbol{x}_0) = \boldsymbol{x}_0 + \mathrm{Ext}(\hat{\boldsymbol{\eta}}(\boldsymbol{x}_0, t)|_{\Sigma^0}).$$

A classical choice is to consider a harmonic extension operator in the reference domain. This mapping does not necessarily track the fluid particles far from the interface Σ^t.

For any function $\hat{g} : \Omega_s^0 \times (0,T) \to \mathbb{R}$ defined in the reference solid configuration, we denote by $g = \hat{g} \circ (\mathscr{L}^t)^{-1}$ its counterpart in the current domain:

$$g : \Omega_s^t \times (0,T) \to \mathbb{R}, \quad g(\boldsymbol{x}, t) = \hat{g}((\mathscr{L}^t)^{-1}(\boldsymbol{x}), t).$$

An analogous notation is adopted for the fluid domain: given $\hat{f} : \Omega_f^0 \times (0,T) \to \mathbb{R}$ defined in the reference fluid configuration, we denote by $f = \hat{f} \circ (\mathscr{A}^t)^{-1}$ its counterpart in the current fluid domain.

We define the ALE time derivative as follows:

$$\partial_t f|_{\boldsymbol{x}_0} : \Omega_f^t \times (0,T) \to \mathbb{R}, \quad \partial_t f|_{\boldsymbol{x}_0}(\boldsymbol{x}, t) = \partial_t \hat{f} \circ (\mathscr{A}^t)^{-1}(\boldsymbol{x}).$$

Moreover, we calculate the fluid domain velocity $\boldsymbol{w}$ as

$$\boldsymbol{w}(\boldsymbol{x}, t) = \partial_t \boldsymbol{x}|_{\boldsymbol{x}_0} = \partial_t \mathscr{A}^t \circ (\mathscr{A}^t)^{-1}(\boldsymbol{x}).$$

The solid is assumed to be an elastic material, characterized by a constitutive law relating the Cauchy stress tensor $\boldsymbol{T}_s$ to the deformation gradient $\boldsymbol{F}(\hat{\boldsymbol{\eta}}) = \boldsymbol{I} + \nabla\hat{\boldsymbol{\eta}}$.

The fluid is assumed to be homogeneous, Newtonian and incompressible. We denote by $\boldsymbol{T}_f$ its Cauchy stress tensor:

$$\boldsymbol{T}_f(\boldsymbol{u}, p) = -p\boldsymbol{I} + 2\mu(\nabla\boldsymbol{u} + (\nabla\boldsymbol{u})^T),$$

where p is the pressure $\boldsymbol{u}$ the velocity and μ the dynamic viscosity.

In order to write the fluid problem in ALE form, let us apply the chain rule to the velocity time derivative:

$$\partial_t \boldsymbol{u}|_{\boldsymbol{x}_0} = \partial_t \boldsymbol{u} + \boldsymbol{w} \cdot \nabla\boldsymbol{u},$$

where $\partial_t \boldsymbol{u}$ is the partial time derivative in the spatial frame (Eulerian derivative).

Then, the fluid–structure problem in strong form reads:

1. *Fluid–structure problem*. Find the fluid velocity $\boldsymbol{u}$, pressure p and the structure displacement $\hat{\boldsymbol{\eta}}$ such that

$$\rho_f \partial_t \boldsymbol{u}|_{\boldsymbol{x}_0} + \rho_f((\boldsymbol{u} - \boldsymbol{w}) \cdot \nabla)\boldsymbol{u} - \nabla \cdot \boldsymbol{T}_f = \boldsymbol{f}_f \quad \text{in } \Omega_f^t \times (0,T), \tag{2a}$$

$$\nabla \cdot \boldsymbol{u} = 0 \quad \text{in } \Omega_f^t \times (0,T), \tag{2b}$$

$$\rho_s \partial_{tt} \hat{\boldsymbol{\eta}} - \nabla \cdot \widehat{\boldsymbol{T}_s} = \widehat{\boldsymbol{f}_s} \quad \text{in } \Omega_s^0 \times (0,T), \tag{2c}$$

$$\boldsymbol{u} = \partial_t \boldsymbol{\eta} \quad \text{on } \Sigma^t \times (0,T), \tag{2d}$$

$$\boldsymbol{T}_s \cdot \boldsymbol{n}_s + \boldsymbol{T}_f \cdot \boldsymbol{n}_f = 0 \quad \text{on } \Sigma^t \times (0,T). \tag{2e}$$

2. *Geometry problem*. Find the fluid domain displacement

$$\mathscr{A}^t(\boldsymbol{x}_0) = \boldsymbol{x}_0 + \mathrm{Ext}(\hat{\boldsymbol{\eta}}|_{\Sigma^0}), \quad \boldsymbol{w} = \partial_t \mathscr{A}^t \circ (\mathscr{A}^t)^{-1}, \quad \Omega_f^t = \mathscr{A}^t(\Omega_f^0). \tag{3}$$

Here, ρ_f and ρ_s are the fluid and structure densities and $\boldsymbol{f}_f$ and $\widehat{\boldsymbol{f}_s}$ the forcing terms. Two transmission conditions are enforced at the interface: the *continuity of fluid and structure velocities* (2d), due to the adherence condition, and the *continuity of normal stresses* (2e), expressing the action–reaction principle. The fluid and structure problems are also coupled by the *geometrical condition* (3), leading to a nonlinear problem. Finally, system (2) and (3) has to be endowed with suitable boundary conditions on $\partial\Omega^t \setminus \Sigma^t$ and initial conditions. Since the choice of boundary and initial conditions is not essential in the forthcoming discussion, they will not be detailed here.

2.2. The time discretization and the algebraic problem

In what follows we discretize in time system (2) and (3). Let Δt be the time step size and $t^n = n\Delta t$ for $n = 0, \ldots, N$. We denote by z^n the approximation of a time dependent function z at time level t^n. Let us define the backward difference operator δ_t as $\delta_t z^{n+1} = (z^{n+1} - z^n)/\Delta t$. The discrete ALE derivative is evaluated by the following expression:

$$\delta_t z^{n+1}|_{\boldsymbol{x}_0} = (z^{n+1} - z^n \circ \mathscr{A}^n \circ (\mathscr{A}^{n+1})^{-1})/\Delta t.$$

We consider a backward Euler scheme for the time discretization of the fluid problem and an implicit first order BDF scheme for the structure problem. Observe, however, that all the partitioned procedures proposed in this work can be easily extended to other, high order, time marching schemes.

In all cases we obtain a nonlinear problem, since the convective term and the interface position are unknown, and possibly the structure is non-linear. Several strategies have been proposed to solve such monolithic problem. To handle all nonlinearities, one could consider *implicit* strategies, obtained for example by a full Newton method (where the tangent operator include shape derivatives, see [15]), by quasi-Newton (for instance by dropping the shape derivatives in the tangent operator, see [20]) or by other fixed-point type iterations where no shape derivatives are involved. Alternatively, one can treat the non-linear terms in an explicit way by extrapolation from previous time steps (*semi-implicit* algorithm, see, e.g., [14,30,4]). Whatever strategy is adopted, a sequence of linearized FSI problems (implicitly coupled through the interface conditions (2d) and (2e)) has to be solved.

Let us now consider the algebraic counterpart of such linearized problem. To this aim, let Ω^* be the (known) domain where this problem is solved. Ω^* is the domain obtained at the previous subiteration in the fixed point loop if an implicit treatment of the interface position is considered, while it is a suitable extrapolation of fluid domains from previous time steps if a semi-implicit algorithm is applied. We introduce a suitable triangulation of the FSI domain Ω^* (for the sake of simplicity assumed conforming at the interface Σ^*) and consider a finite element discretization in space. For the sake of exposition we skip the details and we refer the reader to [4].

By this procedure, we are led at each time step to the solution of the following linear system of equations

$$\begin{bmatrix} C_{ff} & C_{f\Sigma} & 0 & 0 \\ 0 & M_\Sigma & -M_\Sigma & 0 \\ C_{\Sigma f} & C_{\Sigma\Sigma} & N_{\Sigma\Sigma} & N_{\Sigma s} \\ 0 & 0 & N_{s\Sigma} & N_{ss} \end{bmatrix} \begin{bmatrix} \mathbf{V}_f \\ \mathbf{V}_\Sigma \\ \mathbf{U}_\Sigma \\ \mathbf{U}_s \end{bmatrix} = \begin{bmatrix} \mathbf{b}_f \\ \mathbf{0} \\ \mathbf{b}_\Sigma \\ \mathbf{b}_s \end{bmatrix}, \tag{4}$$

where we have split the degrees of freedom associated to nodes interior to the fluid and structure domain from the degrees of freedom associated to the FSI interface and we have omitted the time step superscript for simplicity. The vector $\mathbf{V}_f$ contains interior velocity values and all the pressure values for the fluid, $\mathbf{U}_s$ contains interior velocity values for the structure problem, whereas $\mathbf{V}_\Sigma$ and $\mathbf{U}_\Sigma$ contain the interface velocity values for the fluid and for the structure, respectively.

The first row is the fully discrete version of the momentum and mass conservation equations for the fluid problem in the interior nodes, while the second row states the continuity of the velocities at the interface. Indeed, we have indicated by M_Σ the interface mass matrix, which is invertible, so that the second equation is

equivalent to $\mathbf{V}_\Sigma = \mathbf{U}_\Sigma$. The third equation enforces continuity of normal stresses in a weak form. Finally, the fourth row is the structure problem in the interior nodes.

The right-hand side (RHS) includes time derivative terms, body forces and other terms which come from the fact that the structure problem has been rewritten in terms of velocities instead of displacements.

2.3. The interface problem

As suggested in [11,27] the FSI problem can also be understood as an interface problem in which the only unknown is the velocity at the fluid–structure interface. At the continuous level, the interface problem can be written using the fluid and structure Steklov–Poincaré operators (see e.g. [11]). For the fully discrete FSI system, the interface problem is obtained by means of the fluid and structure Schur complement matrices (discrete versions of the Steklov–Poincaré operators, see [3]). System (4) is equivalent to

$$(\widetilde{C}_\Sigma + \widetilde{N}_\Sigma)\mathbf{U}_\Sigma = \tilde{\mathbf{b}}_\Sigma, \tag{5}$$

where

$$\widetilde{C}_\Sigma = C_{\Sigma\Sigma} - C_{\Sigma f}C_{ff}^{-1}C_{f\Sigma}, \tag{6a}$$

$$\widetilde{N}_\Sigma = N_{\Sigma\Sigma} - N_{\Sigma s}N_{ss}^{-1}N_{s\Sigma} \tag{6b}$$

are the fluid and structure Schur complement matrices and

$$\widetilde{\mathbf{b}}_\Sigma = \mathbf{b}_\Sigma - C_{\Sigma f}C_{ff}^{-1}\mathbf{b}_f - N_{\Sigma s}N_{ss}^{-1}\mathbf{b}_s$$

is the corresponding body force for the interface problem.

It is well known (see e.g. [37]) that for finite element approximation the system matrix of the interface problem (5) has a condition number of order $\mathcal{O}(h^{-1})$ whereas the one for the global system matrix in (4) is $\mathcal{O}(h^{-2})$. Anyway, this matrix is still ill-conditioned and an optimal preconditioner that will cure the dependence of the condition number of the matrix with respect to the mesh size is required. The development of preconditioners for interface problems is one of the main goals of domain decomposition theory (see e.g. [37]). We refer to [11] for an extension of the domain decomposition theory to fluid–structure interaction problems.

In particular, it has been shown in [11] that the classical partitioned procedure known as the Dirichlet–Neumann scheme (see, e.g., [32,29]) can be interpreted as a Richardson method over the preconditioned system

$$\widetilde{N}_\Sigma^{-1}(\widetilde{C}_\Sigma + \widetilde{N}_\Sigma)\mathbf{U}_\Sigma = \widetilde{N}_\Sigma^{-1}\tilde{\mathbf{b}}_\Sigma \tag{7}$$

the preconditioner being $P_{DN} = \widetilde{N}_\Sigma$. In what follows, we refer to this scheme as DN-Richardson. It is well known that this method is *optimal* with respect to h since the condition number of the preconditioned matrix is uniform with respect to the characteristic mesh size h (see [37]). However, for the heterogeneous domain decomposition encountered in FSI, the efficiency of this preconditioner strongly depends on the fluid and structure physical parameters and the time step size (see e.g. [9]). In particular, the performance of the preconditioner deteriorates when the ratio ρ_s/ρ_f decreases (increasing the *added-mass effect*, see [41,9,18]), or when slender domains are considered. Therefore, an optimal preconditioner for the FSI interface problem has to be optimal also with respect to the added-mass effect.

Alternatively to Richardson iterations, one could use more efficient algorithms. In particular, it is possible to consider Krylov methods over the preconditioned system (7) (see [27]). As in [3] we will focus in this work on the GMRES method. Every iteration of this algorithm requires a matrix–vector multiplication with the system matrix $\widetilde{N}_\Sigma^{-1}(\widetilde{N}_\Sigma + \widetilde{C}_\Sigma)$. This matrix–vector product can be easily computed in a modular way if one disposes of separate fluid and structure codes. In [3] it has been shown that the DN preconditioner combined with GMRES iterations (DN-GMRES) performs much better than DN-Richardson for large added-mass effects. However, its performance is still negatively affected by the added-mass and by the time step size.

In [2] a new family of partitioned procedures, based on Robin transmission conditions, has been introduced. Some of these schemes look very attractive, since their dependence on the added-mass effect is limited, as revealed by the convergence analysis and numerical tests proposed therein. In the next section, we interpret these partitioned schemes as preconditioned Richardson iterations on the interface problem and identify the corresponding RR preconditioner to be used later with more efficient Krylov solvers (such as GMRES).

3. The Robin–Robin preconditioners

Let us recall the *sequential Robin–Robin* partitioned scheme for the solution of 4 introduced in [2]. For general sequential Robin–Robin schemes in the framework of domain decomposition we refer, e.g., to [26,1,19]. This algorithm is suitable for problems with large added-mass effect, such as in hemodynamic applications (blood-vessel systems). Both fluid and structure sub-problems are supplemented with Robin transmission conditions, obtained by linear combinations of the interface conditions with coefficients α_f and α_s, respectively. The choice of the coefficients in these combinations is crucial to achieve good convergence properties. A possible choice that provides very good performance in hemodynamic applications has been proposed in [2] and has been obtained starting from the simplified fluid and structure models presented in [9,30], respectively. By setting $\alpha_s = \infty$ or $\alpha_s = 0$ in the structure problem, one recovers other coupling strategies, namely Robin–Dirichlet and Robin–Neumann, respectively. Among all possible choices, the Robin–Neumann algorithm turns out to be the most efficient (see [2]). In particular, it is much more efficient than the classical Dirichlet–Neumann scheme in problems with large added-mass effects. However, for completeness, in the next section we discuss the more general Robin–Robin approach.

The sequential Robin–Robin scheme consists of the following steps:

Algorithm 1: Sequential Robin–Robin

Let k be the iteration index. Given $(\mathbf{U}_\Sigma^k, \mathbf{U}_s^k)$ and the quantities at the previous time steps, we solve

1. Fluid sub-problem (Robin)

$$\begin{bmatrix} C_{ff} & C_{f\Sigma} \\ C_{\Sigma f} & C_{\Sigma\Sigma} + \alpha_f M_\Sigma \end{bmatrix} \begin{bmatrix} \mathbf{V}_f^{k+1} \\ \mathbf{V}_\Sigma^{k+1} \end{bmatrix} = \begin{bmatrix} \mathbf{b}_f \\ \mathbf{b}_\Sigma \end{bmatrix} - \begin{bmatrix} \mathbf{0} \\ N_{\Sigma s}\mathbf{U}_s^k + (N_{\Sigma\Sigma} - \alpha_f M_\Sigma)\mathbf{U}_\Sigma^k \end{bmatrix}. \tag{8a}$$

2. Structure sub-problem (Robin)

$$\begin{bmatrix} N_{\Sigma\Sigma} + \alpha_s M_\Sigma & N_{\Sigma s} \\ N_{s\Sigma} & N_{ss} \end{bmatrix} \begin{bmatrix} \mathbf{U}_\Sigma^{k+1} \\ \mathbf{U}_s^{k+1} \end{bmatrix} = \begin{bmatrix} \mathbf{b}_\Sigma \\ \mathbf{b}_s \end{bmatrix} - \begin{bmatrix} C_{\Sigma f}\mathbf{V}_f^{k+1} + (C_{\Sigma\Sigma} - \alpha_s M_\Sigma)\mathbf{V}_\Sigma^{k+1} \\ \mathbf{0} \end{bmatrix} \tag{8b}$$

with $\alpha_f, \alpha_s > 0$, and iterate until convergence on $(\mathbf{U}_\Sigma^k, \mathbf{U}_s^k)$.

Let us now reinterpret this scheme as preconditioned Richardson iterations over system (5).

We have the following:

Lemma 1. *The sequential Robin–Robin scheme (8) is equivalent to solve the interface problem (5) using preconditioned Richardson iterations with preconditioner*

$$P_{\mathrm{RR}} = \frac{1}{\alpha_f + \alpha_s}(\widetilde{C}_\Sigma + \alpha_f M_\Sigma) M_\Sigma^{-1} (\widetilde{N}_\Sigma + \alpha_s M_\Sigma). \tag{9}$$

Proof. Every preconditioned Richardson iteration of the method consists of: given $\mathbf{U}_\Sigma^k$ compute $\mathbf{U}_\Sigma^{k+1}$ such that

$$\frac{1}{\alpha_f + \alpha_s}(\widetilde{C}_\Sigma + \alpha_f M_\Sigma) M_\Sigma^{-1} (\widetilde{N}_\Sigma + \alpha_s M_\Sigma) \delta\mathbf{U}_\Sigma^{k+1} = \tilde{\mathbf{b}}_\Sigma - (\widetilde{C}_\Sigma + \widetilde{N}_\Sigma)\mathbf{U}_\Sigma^k, \tag{10}$$

where $\delta\mathbf{U}_\Sigma^{k+1} = \mathbf{U}_\Sigma^{k+1} - \mathbf{U}_\Sigma^k$. We can split (10) into two different steps

$$(\widetilde{C}_\Sigma + \alpha_f M_\Sigma)\delta\mathbf{V}_\Sigma^{k+1} = \tilde{\mathbf{b}}_\Sigma - (\widetilde{C}_\Sigma + \widetilde{N}_\Sigma)\mathbf{U}_\Sigma^k, \tag{11a}$$

$$(\widetilde{N}_\Sigma + \alpha_s M_\Sigma)\delta\mathbf{U}_\Sigma^{k+1} = (\alpha_f + \alpha_s) M_\Sigma \delta\mathbf{V}_\Sigma^{k+1}. \tag{11b}$$

Setting now $\delta\mathbf{V}^{k+1} = \mathbf{V}_\Sigma^{k+1} - \mathbf{U}_\Sigma^k$ and rearranging (11a), we have

$$(\widetilde{C}_\Sigma + \alpha_f M_\Sigma)\mathbf{V}_\Sigma^{k+1} = \tilde{\mathbf{b}}_\Sigma - (\widetilde{N}_\Sigma - \alpha_f M_\Sigma)\mathbf{U}_\Sigma^k. \tag{12}$$

Using the definitions (6b) in (12), we get

1. Auxiliary structure sub-problem (Dirichlet)

$$N_{ss}\widetilde{\mathbf{U}}_s^{k+1} = \mathbf{b}_s - N_{s\Sigma}\mathbf{U}_\Sigma^k.$$

2. Fluid sub-problem (Robin)

$$\begin{bmatrix} C_{ff} & C_{f\Sigma} \\ C_{\Sigma f} & C_{\Sigma\Sigma} + \alpha_f M_\Sigma \end{bmatrix} \begin{bmatrix} \mathbf{V}_f^{k+1} \\ \mathbf{V}_\Sigma^{k+1} \end{bmatrix} = \begin{bmatrix} \mathbf{b}_f \\ \mathbf{b}_\Sigma \end{bmatrix} - \begin{bmatrix} \mathbf{0} \\ N_{\Sigma s}\widetilde{\mathbf{U}}_s^{k+1} + (N_{\Sigma\Sigma} - \alpha_f M_\Sigma)\mathbf{U}_\Sigma^k \end{bmatrix}.$$

On the other hand, using (12) and (11b) we get:

$$\begin{aligned}(\widetilde{N}_\Sigma + \alpha_s M_\Sigma)\mathbf{U}_\Sigma^{k+1} &= (\widetilde{N}_\Sigma + \alpha_s M_\Sigma)(\mathbf{U}_\Sigma^k + \delta\mathbf{U}_\Sigma^{k+1}) \\ &= (\widetilde{N}_\Sigma + \alpha_s M_\Sigma)\mathbf{U}_\Sigma^k + (\alpha_f + \alpha_s) M_\Sigma \delta\mathbf{V}_\Sigma^{k+1} \\ &= (\widetilde{N}_\Sigma - \alpha_f M_\Sigma)\mathbf{U}_\Sigma^k + (\alpha_f + \alpha_s) M_\Sigma \mathbf{V}_\Sigma^{k+1} \\ &= \tilde{\mathbf{b}}_\Sigma - (\widetilde{C}_\Sigma + \alpha_f M_\Sigma)\mathbf{V}_\Sigma^{k+1} + (\alpha_f + \alpha_s) M_\Sigma \mathbf{V}_\Sigma^{k+1} \\ &= \tilde{\mathbf{b}}_\Sigma - (\widetilde{C}_\Sigma - \alpha_s M_\Sigma)\mathbf{V}_\Sigma^{k+1},\end{aligned}$$

which corresponds to

(3) Structure sub-problem (Robin)

$$\begin{bmatrix} N_{\Sigma\Sigma} + \alpha_s M_\Sigma & N_{\Sigma s} \\ N_{s\Sigma} & N_{ss} \end{bmatrix} \begin{bmatrix} \mathbf{U}_\Sigma^{k+1} \\ \mathbf{U}_s^{k+1} \end{bmatrix} = \begin{bmatrix} \mathbf{b}_\Sigma \\ \mathbf{b}_s \end{bmatrix} - \begin{bmatrix} C_{\Sigma f}\mathbf{V}_f^{k+1} + (C_{\Sigma\Sigma} - \alpha_s M_\Sigma)\mathbf{V}_\Sigma^{k+1} \\ \mathbf{0} \end{bmatrix}.$$

Observe that the second equation of the third step and the first step coincide. Then, the solution of the auxiliary problem is simply $\widetilde{\mathbf{U}}_s^{k+1} = \mathbf{U}_s^k$. Moreover, if we set $\widetilde{\mathbf{U}}_s^1 = \mathbf{U}_s^{\mathrm{old}}$, with $\mathbf{U}_s^{\mathrm{old}}$ the solution at the previous time step, the auxiliary problem can be eliminated at all. Thus the Richardson algorithm preconditioned with (9) coincides with (8). □

We point out that the preconditioner P_{RR} is called sequential because fluid and structure Robin sub-problems must be performed in a sequential fashion. In what follows, we refer to this scheme as *RR-Richardson*.

Remark 1. An alternative version of the RR preconditioner, introduced in context of domain decomposition methods, can be obtained as a natural extension of the Neumann–Neumann (NN) preconditioner (see [12,21]). Applied to the FSI problem (5) it is defined as:

$$P_{\mathrm{RR}}^{\parallel} = (\beta(\widetilde{C}_\Sigma + \alpha_f M_\Sigma)^{-1} + (1-\beta)(\widetilde{N}_\Sigma + \alpha_s M_\Sigma)^{-1})^{-1},$$

where $\beta \in (0,1)$ is arbitrary and affects the convergence rate (*parallel RR preconditioner*). It entails the solution of two fluid and two structure sub-problems at each iteration. However, the numerical results obtained for this method are fairly disappointing and have not been included.

4. RR-preconditioned GMRES method

The reinterpretation of the RR partitioned procedures as preconditioned Richardson iterations on the interface system is not just formal. It allows us to use more efficient (orthonormal) Krylov methods on the (preconditioned) interface problem instead of Richardson iterations (see [3] for the DN algorithm). In particular, we can consider the GMRES algorithm, obtaining the RR-GMRES scheme. In order to do that, we have to generate the Krylov basis associated to the matrix $Q = P_{\mathrm{RR}}^{-1}(\widetilde{C}_\Sigma + \widetilde{N}_\Sigma)$, started with the initial preconditioned residual $\mathbf{r}^0 = P_{\mathrm{RR}}^{-1}[\tilde{\mathbf{b}}_\Sigma - (\widetilde{C}_\Sigma + \widetilde{N}_\Sigma)\mathbf{U}_\Sigma^0]$, where $\mathbf{U}_\Sigma^0$ is the initial guess for the interface velocity. The Krylov space that is generated at the mth iteration of the GMRES method is

$$\mathscr{K}_m := \mathrm{span}\{\mathbf{r}^0, Q\mathbf{r}^0, Q^2\mathbf{r}^0, \ldots, Q^{m-1}\mathbf{r}^0\}.$$

In fact, the GMRES method uses an orthonormal basis $\{\mathbf{z}^j\}$ such that

$$\mathrm{span}\{\mathbf{z}^0, \mathbf{z}^1, \ldots, \mathbf{z}^{m-1}\} = \mathscr{K}_m.$$

Given $\mathbf{z}^k$, in order to get $\mathbf{z}^{k+1}$ we have to evaluate a matrix–vector product

$$\mathbf{w} = P_{\mathrm{RR}}^{-1}(\widetilde{N}_\Sigma + \widetilde{C}_\Sigma)\mathbf{z}^k, \tag{13}$$

and then compute $\mathbf{z}^{k+1} = \mathbf{w} - \Pi_{\mathscr{K}_M}\mathbf{w}$, where $\Pi_{\mathscr{K}_M}$ is the orthogonal projection operator onto $\mathscr{K}_M$.

For the sequential RR preconditioner, the following result holds:

Lemma 2. *The matrix–vector product (13) can be rearranged in the following three steps:*

$$(\widetilde{C}_\Sigma + \alpha_f M_\Sigma)\tilde{\mathbf{v}}_\Sigma = (\widetilde{N}_\Sigma - \alpha_f M_\Sigma)\mathbf{z}^k, \tag{14a}$$

$$(\widetilde{N}_\Sigma + \alpha_s M_\Sigma)\mathbf{v}_\Sigma = (\widetilde{C}_\Sigma - \alpha_s M_\Sigma)\tilde{\mathbf{v}}_\Sigma, \tag{14b}$$

$$\mathbf{w} = \mathbf{z}^k - \mathbf{v}_\Sigma. \tag{14c}$$

Proof. From (14a) and (14b), we have

$$\mathbf{v}_\Sigma = (\widetilde{N}_\Sigma + \alpha_s M_\Sigma)^{-1}(\widetilde{C}_\Sigma - \alpha_s M_\Sigma)(\widetilde{C}_\Sigma + \alpha_f M_\Sigma)^{-1}(\widetilde{N}_\Sigma - \alpha_f M_\Sigma)\mathbf{z}^k.$$

Then, from (14c), we obtain

$$\begin{aligned}\mathbf{w} &= [I - (\widetilde{N}_\Sigma + \alpha_s M_\Sigma)^{-1}(\widetilde{C}_\Sigma - \alpha_s M_\Sigma)(\widetilde{C}_\Sigma + \alpha_f M_\Sigma)^{-1}(\widetilde{N}_\Sigma - \alpha_f M_\Sigma)]\mathbf{z}^k \\ &= (\widetilde{N}_\Sigma + \alpha_s M_\Sigma)^{-1}[(\alpha_s + \alpha_f) M_\Sigma \\ &\quad + (\alpha_s + \alpha_f) M_\Sigma (\widetilde{C}_\Sigma + \alpha_f M_\Sigma)^{-1}(\widetilde{N}_\Sigma - \alpha_f M_\Sigma)]\mathbf{z}^k \\ &= P_{\mathrm{RR}}^{-1}(\widetilde{N}_\Sigma + \widetilde{C}_\Sigma)\mathbf{z}^k\end{aligned}$$

with P_{RR} as in (9). □

We can rewrite the matrix–vector product (13) as a set of sub-problems. In particular, the first two equations in (14) leads to the following

Algorithm 2: Sequential Robin–Robin GMRES (matrix–vector multiplication)

1. Auxiliary structure sub-problem (Dirichlet)

$$N_{ss}\tilde{\mathbf{v}}_s = -N_{s\Sigma}\mathbf{z}^k.$$

Table 1
Sub-problems characterizing the different algorithms: R and D indicate that the sub-problem is equipped with a Robin or a Dirichlet boundary condition at the interface.

	Richardson	GMRES
P_{RR}	Fluid 1R – Struct. 1R	Fluid 1R – Struct. 1D + 1R
$P^{\parallel}_{RR}$	Fluid 1D + 1R – Struct. 1D+1R	Fluid 1D + 1R – Struct. 1D + 1R

2. Fluid sub-problem (Robin)

$$\begin{bmatrix} C_{ff} & C_{f\Sigma} \\ C_{\Sigma f} & C_{\Sigma\Sigma}+\alpha_f M_\Sigma \end{bmatrix} \begin{bmatrix} \tilde{\mathbf{v}}_f \\ \tilde{\mathbf{v}}_\Sigma \end{bmatrix} = \begin{bmatrix} 0 \\ N_{\Sigma s}\tilde{\mathbf{v}}_s + (N_{\Sigma\Sigma}-\alpha_f M_\Sigma)\mathbf{z}^k \end{bmatrix}.$$

3. Structure sub-problem (Robin)

$$\begin{bmatrix} N_{\Sigma\Sigma}+\alpha_s M_\Sigma & N_{\Sigma s} \\ N_{s\Sigma} & N_{ss} \end{bmatrix} \begin{bmatrix} \mathbf{v}_\Sigma \\ \mathbf{v}_s \end{bmatrix} = \begin{bmatrix} C_{\Sigma f}\tilde{\mathbf{v}}_f + (C_{\Sigma\Sigma}-\alpha_s M_\Sigma)\tilde{\mathbf{v}}_\Sigma \\ 0 \end{bmatrix}.$$

We point out that the auxiliary structure sub-problem arises from the matrix–vector product $\widetilde{N}_\Sigma \mathbf{z}^k$ which involves the product $N_{ss}^{-1}N_{s\Sigma}\mathbf{z}^k$, that is a structure problem with Dirichlet boundary conditions. The same occurs for the matrix–vector product $\widetilde{C}_\Sigma\tilde{\mathbf{v}}_\Sigma$ that involves a fluid sub-problem with Dirichlet boundary conditions. However, in this case we have $C_{ff}^{-1}C_{f\Sigma}\tilde{\mathbf{v}}_\Sigma = \tilde{\mathbf{v}}_f$ and this sub-problem can be skipped.

From a computational point of view, the extra cost of one GMRES iteration (matrix–vector multiplication (13)) with respect to one Richardson iteration is given by the auxiliary structure problem in step (1), which must be solved and cannot be avoided (as done in Lemma 1 for the Richardson iterations). Note that also DN-GMRES requires only two sub-problems per iterations (see [3]). In any case, the extra sub-problem is a structural one, which in most real applications (such as in hemodynamics) is much cheaper than the fluid one.

In conclusion, we can compute the matrix–vector product (13), which allows us to build the new basis element of the Krylov space, by solving the same systems that appear when using Richardson iterations, the only modification being the extra auxiliary structure sub-problem.

Remark 2. The last step (Robin problem for the structure) could be replaced by

$$(\widetilde{N}_\Sigma + \alpha_s M_\Sigma)\mathbf{w} = (\alpha_f+\alpha_s)(\tilde{\mathbf{v}}_\Sigma + \mathbf{z})$$

slightly reducing the computational cost.

In Table 1 we indicate the sub-problems that have to be solved at each iteration for the methods considered.

5. On the modularity of the RR algorithms

In [2] we pointed out the modularity of the sequential RR-Richardson scheme, that is the possibility of using "black-box" fluid and structure solvers. Here, we want to stress that also the sequential RR-GMRES schemes is modular.

The building block of all algorithms presented so far (Algorithms 1 and 2) is the solution of Robin problems as (8a) and (8b). Our goal is to show that all quantities appearing in (8a) are easily accessible when using "black-box" fluid and structure solvers. Therefore, the proposed algorithms are actually *modular*.

Let us split the boundary forcing term in (8a) as $\mathbf{b}_\Sigma = \mathbf{b}_\Sigma^f + \mathbf{b}_\Sigma^s$ and assume that the term $\mathbf{U}_s$ satisfies the algebraic system (as it is the case in Algorithms 1 and 2)

$$N_{ss}\mathbf{U}_s = \mathbf{b}_s - N_{s\Sigma}\mathbf{U}_\Sigma$$

corresponding to a Dirichlet structure problem. The residual of the structure equation on the interface nodes, given in algebraic form by

$$R(\mathbf{b}_s, \mathbf{U}_s, \mathbf{U}_\Sigma) = N_{\Sigma s}\mathbf{U}_s + N_{\Sigma\Sigma}\mathbf{U}_\Sigma - \mathbf{b}_\Sigma^s$$

represents the structure normal stress at the interface in a weak form (i.e. already integrated against the structure shape functions corresponding to the interface degrees of freedom, see e.g. [4]). Hence, system (8a) can be rewritten as

$$\begin{bmatrix} C_{ff} & C_{f\Sigma} \\ C_{\Sigma f} & C_{\Sigma\Sigma}+\alpha_f M_\Sigma \end{bmatrix} \begin{bmatrix} \mathbf{V}_f \\ \mathbf{V}_\Sigma \end{bmatrix} = \begin{bmatrix} \mathbf{b}_f \\ \mathbf{b}_\Sigma^f \end{bmatrix} - \begin{bmatrix} \mathbf{0} \\ R(\mathbf{b}_s, \mathbf{U}_s, \mathbf{U}_\Sigma) - \alpha_f M_\Sigma \mathbf{U}_\Sigma \end{bmatrix}. \tag{15}$$

Let us denote by $\dot{\boldsymbol{\eta}}_h$ the finite element function whose nodal values are given by the vectors $(\mathbf{U}_s, \mathbf{U}_\Sigma)$ (structure velocity), $\boldsymbol{\eta}_h$ the corresponding structure displacement, and $(\boldsymbol{u}_h, p_h)$ the finite element fluid functions corresponding to the vectors $(\mathbf{V}_f, \mathbf{V}_\Sigma)$. It is easy to see that system (15) corresponds to a standard fluid problem with the following Robin boundary conditions at the interface:

$$\alpha_f \boldsymbol{u}_h + \boldsymbol{T}_f(\boldsymbol{u}_h, p_h)\cdot\boldsymbol{n}_f = -\boldsymbol{T}_s(\boldsymbol{\eta}_h)\cdot\boldsymbol{n}_s + \alpha_f\dot{\boldsymbol{\eta}}_h.$$

Exactly the same considerations apply to the structure Robin problem (8b). We see that the algorithms we have proposed so far are *modular* provided we dispose of fluid and structure solvers that allow us to impose Robin boundary conditions with non-zero right hand side and that can output the velocity and normal stress on the interface, information that has to be passed to the other sub-problem.

6. Analysis of a model problem

In this section, we analyze the convergence of the RN-GMRES algorithm for a FSI model problem and compare its reduction factor to the one found in [3] for DN-GMRES (see also [28] for a numerical investigation of DN-GMRES in the compressible case). The RN-GMRES scheme is obtained from the general RR-GMRES setting $\alpha_s = 0$. The simplified FSI model considered here has been previously introduced in [9] for the analysis of the DN-Richardson scheme. We refer to [9,2] for the analysis of DN-Richardson scheme, to [3] for the analysis of DN-GMRES and to [2] for the analysis of RN-Richardson.

The model problem is a simplified blood-vessel system. We take a rectangular fluid domain $\Omega^f \in \mathbb{R}^2$ of height R and length L (see Fig. 2), which will be considered fixed in time.

The structure is placed on the top side of Ω^f and is considered a one-dimensional body, that is $\Omega_s \equiv \Sigma$, where Σ denotes the (fixed) fluid–structure interface. We assume that it is described by the generalized string model (see e.g. [36]) and that only normal displacements are possible. The model for the fluid is linear, incompressible and inviscid. The fluid problem is discretized in time by using the implicit backward Euler scheme. A first order BDF scheme is considered for the structure. Then, the FSI coupled problem, discretized in time reads as:

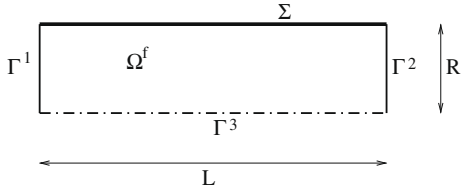

Fig. 2. Reference domains Ω_f.

$$\rho_f \delta_t \boldsymbol{u} + \nabla p^{n+1} = \boldsymbol{0} \quad \text{in } \Omega^f \times (0,T), \tag{16a}$$

$$\nabla \cdot \boldsymbol{u} = 0 \quad \text{in } \Omega^f \times (0,T), \tag{16b}$$

$$\boldsymbol{u} \cdot \boldsymbol{n}_f = \delta_t \eta^{n+1} \quad \text{on } \Sigma \times (0,T), \tag{16c}$$

$$\rho_s H_s \frac{\eta^{n+1} - 2\eta^n + \eta^{n-1}}{\Delta t^2} + a\eta^{n+1} - b\partial_{xx}\eta^{n+1} = p^{n+1} \quad \text{in } \Omega^s \times (0,T), \tag{16d}$$

with suitable boundary conditions on $\Omega^f \setminus \Sigma$. Here, $\eta = \eta(x,t)$ is the displacement in the direction of $\boldsymbol{n}^f$, H_s is the thickness of the structure, $a = EH_s/R^2(1-\nu^2)$, E being the Young modulus and ν the Poisson coefficient, $b = kGH_s$, G being the shear stress modulus and k the Timoshenko shear correction factor. We observe that the continuity of the normal stress at the interface is given by the structure equation itself. In [9,2], it has been shown that the previous problem can be reduced to the following interface equation

$$(\rho_s H_s \mathscr{I} + \rho_f \mathscr{M}) \frac{\eta^{n+1} - 2\eta^n + \eta^{n-1}}{\Delta t^2} + a\eta^{n+1} + \mathscr{N}\eta^{n+1} = \hat{p}^{n+1} \quad \text{in } \Omega^s \times (0,T),$$

where $\mathscr{I}$ is the identity operator, $\hat{p}^{n+1}$ takes into account non-homogeneous boundary conditions on $\partial\Omega_f \setminus \Sigma$ and $\mathscr{M} : H^{-1/2}(\Sigma) \to H^{1/2}(\Sigma)$ stands for the *added-mass* operator which consists of: given $\gamma \in H^{-1/2}(\Sigma)$, find $q \in H^1(\Omega^f)$ such that

$$-\Delta q = 0 \quad \text{in } \Omega^f,$$
$$q = 0 \quad \text{on } \Gamma^1 \cup \Gamma^2,$$
$$\frac{\partial q}{\partial \boldsymbol{n}} = 0 \quad \text{on } \Gamma^3,$$
$$\frac{\partial q}{\partial \boldsymbol{n}} = \gamma \quad \text{on } \Sigma.$$

and extract the value of the solution q on Σ. Moreover, $\mathscr{N} = -\partial_{xx}$. We refer to [9] for a more detailed illustration of the model problem under consideration We can write the interface problem in more compact form as

$$\mathscr{Q}\eta^{n+1} = f_\Sigma^{n+1},$$

where the operator $\mathscr{Q}$ is given by

$$\mathscr{Q} = \left(\frac{\rho_s H_s}{\Delta t} + a\Delta t\right)\mathscr{I} + b\Delta t\mathscr{N} + \frac{\rho_f}{\Delta t}\mathscr{M}$$

and f_Σ includes all the forcing terms. We will not detail it since its expression does not play any role in the subsequent analysis.

We can split $\mathscr{Q}$ into its fluid and structure contributions, $\mathscr{Q}_f$ and $\mathscr{Q}_s$ respectively:

$$\mathscr{Q}_f = \frac{\rho_f}{\Delta t}\mathscr{M}, \quad \mathscr{Q}_s = \left(\frac{\rho_s H_s}{\Delta t} + a\Delta t\right)\mathscr{I} + b\Delta t\mathscr{N}.$$

Then, the RN-GMRES consists of applying the GMRES algorithm over the preconditioned interface problem

$$\mathscr{P}_{RN}^{-1}\mathscr{Q}\eta^{n+1} = \mathscr{P}_{RN}^{-1} f_\Sigma^{n+1},$$

where in analogy with (9), the Robin–Neumann preconditioner is

$$\mathscr{P}_{RN} = \frac{1}{\alpha_f}(\mathscr{Q}_f + \alpha_f \mathscr{I})\mathscr{Q}_s.$$

Let us show that operator $\mathscr{P}_{RN}^{-1}\mathscr{Q}$ is symmetric, positive. We observe that the operators $\mathscr{M}$ and $\mathscr{N}$ are symmetric, positive and diagonalize for the $L^2(\Sigma)$ orthonormal basis

$$g_i = \sqrt{\frac{2}{L}}\sin\left(i\pi\frac{x}{L}\right), \quad i = 1,2,\ldots.$$

The associated eigenvalues are

$$\mu_i(\mathscr{M}) = \frac{L}{i\pi\tanh\left(i\pi\frac{R}{L}\right)} \quad \text{and} \quad \lambda_i(\mathscr{N}) = \left(\frac{i\pi}{L}\right)^2, \quad \text{for } i = 1,2,\ldots,$$

respectively (see [9,2]). We also denote by $\psi_i = \rho_f \mu_i/\Delta t$ the eigenvalues of the operator $\mathscr{Q}_f$. Then, first of all we notice that operator $\mathscr{Q}$ is symmetric, positive, satisfying $\mathscr{Q}g_i = (\psi_i + \alpha_f^{\text{opt}} + b\Delta t\lambda_i)g_i$. Moreover, in [2], it has been shown that an optimal choice for the parameter α_f is given by

$$\alpha_f^{\text{opt}} = \frac{\rho_s H_s}{\Delta t} + a\Delta t \tag{17}$$

so that $\mathscr{Q}_s^{-1}g_i = \frac{1}{(b\Delta t\lambda_i + \alpha_f^{\text{opt}})}g_i$ and $(\mathscr{Q}_f + \alpha_f^{\text{opt}}\mathscr{I})^{-1}g_i = \frac{1}{(\psi_i + \alpha_f^{\text{opt}})}g_i$. Then, $\mathscr{P}_{RN}^{-1} = \alpha_f^{\text{opt}}\mathscr{Q}_s^{-1}(\mathscr{Q}_f + \alpha_f^{\text{opt}}\mathscr{I})^{-1}$ is symmetric, positive since $\mathscr{Q}_s^{-1}$ and $(\mathscr{Q}_f + \alpha_f^{\text{opt}}\mathscr{I})^{-1}$ are symmetric, positive, and share the same eigenfunctions. Moreover, $\mathscr{P}_{RN}^{-1}g_i = \frac{\alpha_f^{\text{opt}}}{(\psi_i + \alpha_f^{\text{opt}})(b\Delta t\lambda_i + \alpha_f^{\text{opt}})}g_i$, and therefore also $\mathscr{Q}$ and $\mathscr{P}_{RN}^{-1}$ share the same eigenfunctions g_i, so that also operator $\mathscr{P}_{RN}^{-1}\mathscr{Q}$ is symmetric, positive.

It is known that the residual $\mathbf{r}^{(k)}$ at the current iteration k of GMRES applied to a symmetric, positive operator $\mathscr{R}$ satisfies the following estimate

$$\|\mathbf{r}^{(k)}\| \leqslant \left(1 - \frac{\sigma_{min}}{\sigma_{max}}\right)^{k/2}\|\mathbf{r}^{(0)}\|, \tag{18}$$

where $\mathbf{r}^{(0)}$ is the initial residual and

$$\sigma_{min} = \inf_{\eta \neq 0}\frac{(\mathscr{R}\eta,\eta)}{(\eta,\eta)}, \quad \sigma_{max} = \sup_{\eta \neq 0}\frac{(\mathscr{R}\eta,\eta)}{(\eta,\eta)},$$

(see [40]). In order to compare the effectiveness of different preconditioners, we define an "average" reduction factor between two subsequent iterations, ρ, as

$$\rho := \left(\frac{\|\mathbf{r}^{(k)}\|}{\|\mathbf{r}^{(0)}\|}\right)^{1/k}.$$

Therefore, thanks to (18), ρ satisfies

$$\rho \leqslant \sqrt{1 - \frac{\sigma_{min}}{\sigma_{max}}}. \tag{19}$$

Since we have shown that $\mathscr{P}_{RN}^{-1}\mathscr{Q}$ is symmetric, positive, we can use bound (19) with

$$\sigma_{min} = \inf_{\eta \neq 0}\frac{(\mathscr{P}_{RN}^{-1}\mathscr{Q}\eta,\eta)}{(\eta,\eta)}, \quad \sigma_{max} = \sup_{\eta \neq 0}\frac{(\mathscr{P}_{RN}^{-1}\mathscr{Q}\eta,\eta)}{(\eta,\eta)}.$$

We have the following result:

Proposition 1. *The RN-GMRES method, with the optimal choice α_f^{opt} given in (17), applied to the simplified system (16), always converges to the monolithic solution, with reduction factor bounded by*

$$\rho_{RN} \leqslant \sqrt{\frac{1}{1 + \frac{\rho_s H_s + a\Delta t^2}{b\Delta t^2\lambda_{\bar{i}}} + \frac{\rho_s H_s + a\Delta t^2}{\rho_f \mu_{\bar{i}}} + \frac{(\rho_s H_s + a\Delta t^2)^2}{b\Delta t^2\lambda_{\bar{i}}\rho_f\mu_{\bar{i}}}}}, \tag{20}$$

where $\bar{i} = \text{argmin}_{i=1,2,\ldots}\left\{\frac{b\Delta t\lambda_i\psi_i}{(\psi_i + \alpha_f^{\text{opt}})(b\Delta t\lambda_i + \alpha_f^{\text{opt}})}\right\}$

Proof. Let us evaluate σ_{min} and σ_{max} with the notation introduced above. The operator $\mathscr{P}_{RN}^{-1}\mathscr{Q}$ can be written as

$$\mathscr{P}_{RN}^{-1}\mathscr{Q} = \mathscr{I} - \mathscr{P}_{RN}^{-1}(\mathscr{P}_{RN} - \mathscr{Q}).$$

On the other hand, we have that

$$\mathscr{P}_{RN} = \frac{1}{\alpha_f^{\text{opt}}}(\mathscr{Q}_f + \alpha_f^{\text{opt}}\mathscr{I})(\alpha_f^{\text{opt}}\mathscr{I} + b\Delta t\mathscr{N})$$
$$= \mathscr{Q}_f + \frac{1}{\alpha_f^{\text{opt}}}\mathscr{Q}_f b\Delta t\mathscr{N} + \alpha_f^{\text{opt}}\mathscr{I} + b\Delta t\mathscr{N} = \frac{1}{\alpha_f^{\text{opt}}}\mathscr{Q}_f b\Delta t\mathscr{N} + \mathscr{Q}.$$

Thanks to the last two identities, we get:

$$\mathscr{P}_{RN}^{-1}\mathscr{Q} = \mathscr{I} - \frac{1}{\alpha_f^{\text{opt}}}\mathscr{P}_{RN}^{-1}\mathscr{Q}_f b\Delta t\mathscr{N}.$$

At this point, we can easily evaluate the eigenvalues of $\mathscr{P}_{RN}^{-1}\mathscr{Q}$ associated to g_i, and denoted by γ_i:

$$\mathscr{P}_{RN}^{-1}\mathscr{Q}g_i = \left(1 - \frac{b\Delta t\lambda_i\psi_i}{(\psi_i + \alpha_f^{\text{opt}})(b\Delta t\lambda_i + \alpha_f^{\text{opt}})}\right)g_i := \gamma_i g_i.$$

The supremum of γ_i is attained for $i \to \infty$, and its value is 1. This is due to the fact that $\lambda_i \to \infty$ and $\psi_i \to 0$ as $i \to \infty$. Therefore, $\sigma_{max} = 1$. It is easy to see that $0 < \gamma_i < 1$. However, it does not exhibit a monotone behavior with respect to i. Let us denote by $\bar{i}$ the value of i for which the minimum is attained so that $\sigma_{min} = \gamma_{\bar{i}}$. The reduction factor reads as:

$$\rho_{RN} = \sqrt{1-\gamma_{\bar{i}}} = \sqrt{\frac{b\Delta t\lambda_{\bar{i}}\psi_{\bar{i}}}{(\psi_{\bar{i}} + \alpha_f^{\text{opt}})(b\Delta t\lambda_{\bar{i}} + \alpha_f^{\text{opt}})}}$$
$$= \sqrt{\frac{b\Delta t^2\lambda_{\bar{i}}\rho_f\mu_{\bar{i}}}{(\rho_f\mu_{\bar{i}} + \rho_s H_s + a\Delta t^2)(b\Delta t^2\lambda_{\bar{i}} + \rho_s H_s + a\Delta t^2)}},$$

and the thesis follows. □

The reduction factor for DN-GMRES has been derived in [3] and is given by:

$$\rho_{DN} = \sqrt{\frac{\rho_f\mu_1}{\rho_s H_s + a\Delta t^2 + \Delta t^2 b\lambda_1}}. \tag{21}$$

6.1. Sensitivity analysis of the reduction factors

Let us compare the bounds for the reduction factor ρ of RN-GMRES and DN-GMRES for the physical parameters given in Table 2 with $\Delta t = 4 \times 10^{-4}$. We check the sensitivity of the analytical expression of ρ given in (20) and (21) for the two methods, with respect to some important values: $\rho_f, \rho_s, \Delta t$ and the Young's modulus E. For every parameter, we consider the problem for the reference parameter times a factor in the range $[10^{-4}, 10^4]$. This is a very wide range and extremal values can be of no interest for real applications, but it allows to identify the asymptotic behavior. Let us remark that the reduction factor plots in Figs. 3 and 4 are obtained from its analytical expression and not from numerical experimentation. In the x-coordinate of these plots we have the factor we multiply the reference parameter by.

In order to analyze the sensitivity with respect to the added-mass, we consider variations of the structure density ρ_s. It is clear from Fig. 3a that RN-GMRES is more efficient than DN-GMRES. For the typical range in hemodynamics (factor $\sim$1), the reduction factor for RN-GMRES is around 0.5, whereas it is almost 1 for DN-GMRES. The bad behavior of DN-GMRES in hemodynamics applications has been reported in [3]. Variations of H_s and a have a similar effect on the reduction factor of both methods, as we can see from (20), (21). Let us comment that for aeroelastic applications (factor $\sim 10^2 - 10^3$) both methods are very effective. However, in the whole range of ρ_s, RN-GMRES proves to be more effective than DN-GMRES.

Table 2
Fluid and structure physical properties.

Fluid density: $\rho_f = 1.0$ g/cm^3	Fluid viscosity: $\mu = 0.035$ poise
Structure density: $\rho_s = 1.1$ g/cm^3	Wall thickness: $h = 0.1$ cm
Lamé constants: $\mu_\ell = 10^6$ dyne/cm^2,	$\lambda_\ell = 1.73 \times 10^6$ dyne/cm^2

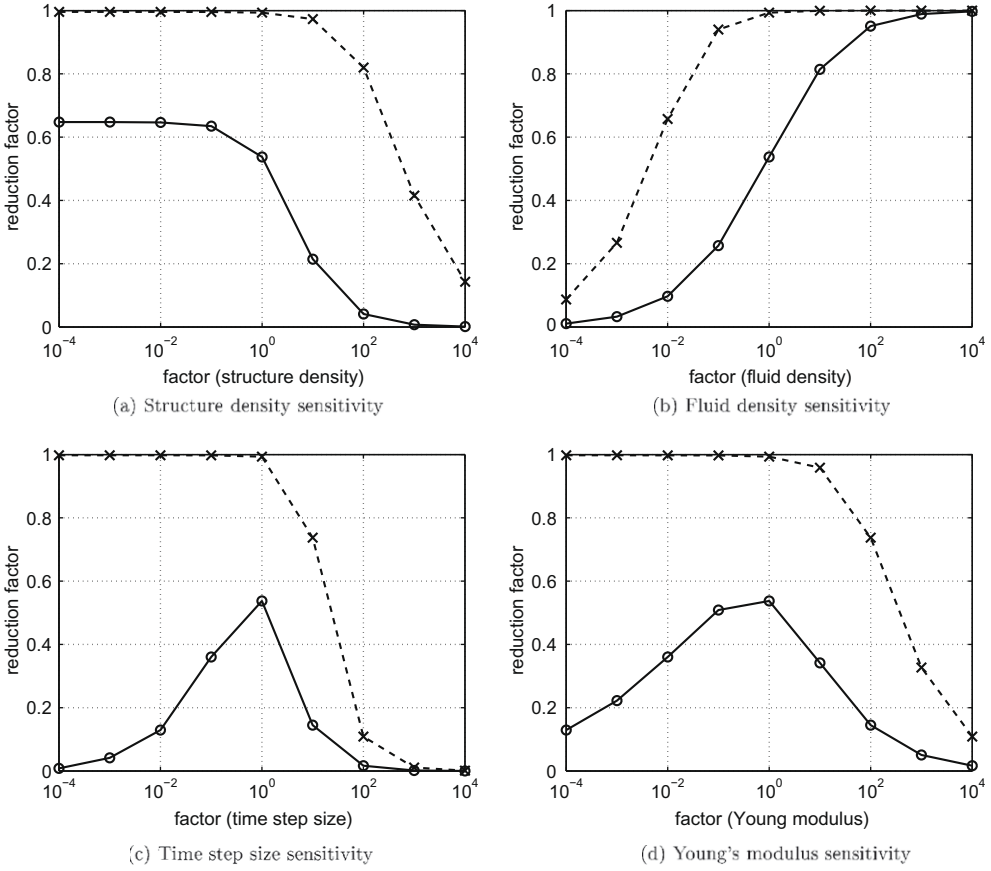

(a) Structure density sensitivity (b) Fluid density sensitivity

(c) Time step size sensitivity (d) Young's modulus sensitivity

Fig. 3. Reduction factor for RN-GMRES (solid line with circles) and for DN-GMRES (dashed line with x) with respect to several parameters. The horizontal scale is relative to a reference value.

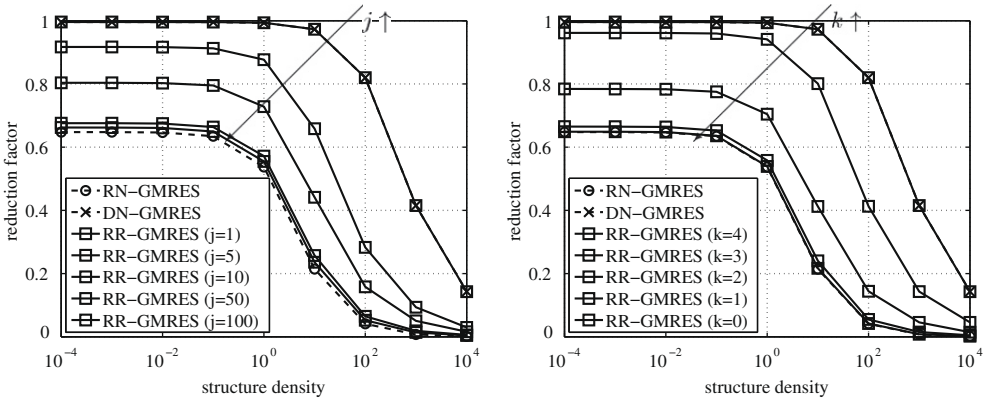

(a) RR for different j and k=0 (b) RR for different k and $j = 1$

Fig. 4. Reduction factor for RN, DN, and RR vs. the factor in $[10^{-4}, 10^{4}]$ that multiplies the structure density ρ_s. For the RR algorithm, we consider different values of j and k in (22).

An alternative way to show the added-mass sensitivity is to play with ρ_f (see Fig. 3b). Again, RN-GMRES always exhibits smaller reduction factor (faster convergence). In this case, for both schemes the reduction factor tends to 1 for extremely large fluid density, as for $\rho_f \sim 1000\rho_s$. However, as far as we know, there are no applications of interest in this ultra-large added-mass range.

Another negative point of the DN-GMRES algorithm is its bad behavior for small time step sizes. In Fig. 3c we solve the FSI problem for different values of Δt. It is clear from this figure that DN-GMRES barely converges as $\Delta t \to 0$. On the contrary, the convergence of RN-GMRES is not deteriorated in the small time step limit. As would be expected from (20), the reduction factor tends to 0 (no iterations needed) very fast in this limit.

Finally, we vary the stiffness of the material, multiplying the reference Young's modulus by a factor in $[10^{-4}, 10^{4}]$. We see in Fig. 3d that DN-GMRES barely converges as the stiffness of the material is reduced. On the contrary, RN-GMRES always converges.

In conclusion, we can state that RN-GMRES scheme exhibits a much better behavior than the DN-GMRES scheme for a wide range of parameters.

We turn now to the more general RR-GMRES algorithm. The reduction factor for RR-GMRES and a generic α_s can be obtained in a similar way as for RN-GMRES. We omit the proof and the expression of the reduction factor in this case. The value of α_s must be a good approximation of the operator $\mathcal{Q}_f$. We consider the following expression (see [2]):

$$\alpha_s = 10^{-k} \frac{\rho_f L}{\Delta t j \pi \tanh\left(j\pi \frac{R}{L}\right)}, \tag{22}$$

where 10^{-k}, $k \geqslant 0$, is a factor smaller than one which multiplies a single eigenvalues of $\mathcal{Q}_f$, for a chosen j (the value $j = 1$ refers to the maximum eigenvalue).

We show in Fig. 4 the reduction factor for RN-GMRES, DN-GMRES and RR-GMRES. For RR-GMRES we have considered a wide set of choices for j and k. The direction of growth of j and k is marked with arrows. It is easily inferred that the reduction factor for RR-GMRES is always smaller than DN-GMRES but larger than RN-GMRES. As expected, the method tends to RN-GMRES as $\alpha_s \to 0$ (that is to say, increasing k and/or j). On the other hand, the algorithm performs as DN-GMRES for the case $k = 0$ and $j = 1$, which consists in taking α_s equal to the maximum eigenvalue of $\mathcal{Q}_f$. As a conclusion, for the model problem, the RN-GMRES algorithm is the optimal choice. For a more realistic problem (where the fluid is governed by the Navier–Stokes equation) and Richardson coupling iterations are performed, a slight improvement of RR-Richardson with respect to RN-Richardson was found in [2] for specific choices of α_s. In any case, finding an appropriate α_s is not easy and the improvements are very small. For this reasons, we will consider only the RN preconditioner in the numerical experiments of Section 8. Anyway, the use of RR algorithms can be of great interest in case of dealing with fully submerged incompressible structures (see Section 7).

7. Enclosed fluid sub-problem

In the previous sections, we did not specify the fluid boundary conditions on $\partial\Omega_f \setminus \Sigma$ because they do not play any role in the design of partitioned procedures. However, there is a pathological case in which these boundary conditions can make the Dirichlet–Neumann partitioned procedures inadequate. Let us assume that the fluid sub-problem is supplemented on $\partial\Omega_f \setminus \Sigma$ with the Dirichlet boundary conditions

$$\boldsymbol{u} \cdot \boldsymbol{n}_f = u_d \quad \text{on } \partial\Omega_f \setminus \Sigma. \tag{23}$$

When using the Dirichlet–Neumann method and the boundary condition (23) is prescribed, the fluid sub-problem is supplemented with Dirichlet boundary conditions on its whole boundary. As a consequence, the fluid matrix becomes singular because the pressure is only determined up to a constant. To overcome this problem, it is possible to fix the value of the pressure in a node or project the pressure equation onto the subspace of functions with zero average. However, the pressure for the original unsplit FSI system is unique, since it is determined by the interaction with the structure.

On the other hand, from the fluid continuity equation, the structure displacement has to satisfy the condition

$$-\int_{\Omega_f} \nabla \cdot \boldsymbol{u} = \int_{\partial\Omega_f \setminus \Sigma} u_d + \int_{\Sigma} \partial_t \boldsymbol{\eta} \cdot \boldsymbol{n}_f = 0. \tag{24}$$

However, there is no guarantee that in the "Neumann" step, the structure solver computes a structure velocity satisfying (24) and if this does not happen, the fluid Dirichlet datum is incompatible, meaning that at the algebraic level, the right hand side of the fluid sub-problem is not admissible. Therefore, an algorithm based on the DN preconditioner cannot be straightforwardly applied in this case.

In the following, we review some existing strategies to overcome this difficulty and finally tackle this problem with the Robin–Robin algorithm.

7.1. Review of existing strategies

One modification of the DN algorithm which makes this algorithm suitable for balloon-type problems has been suggested in [25], by the introduction of a Lagrange multiplier. Here we want to derive the interface problem related to this equation and the corresponding DN-interface preconditioner, in order to extend such a strategy to GMRES iterations.

The system matrix C_{ff} is singular in this case. Indeed, the kernel of this matrix, $\mathrm{Ker}(C_{ff})$, is of dimension one, and a basis is given by the element $[\mathbf{U}_f, \mathbf{P}]^T = [\mathbf{0}, \mathbf{1}]^T$. In order to make the fluid sub-problem well posed (with a uniquely defined pressure), let us introduce the pressure finite-dimensional space $Q_{h,0} \equiv Q_h \setminus \mathrm{Ker}(C_{ff})$ corresponding to pressure functions with zero mean value, and matrix C^0_{ff} obtained by projection of C_{ff} onto $Q_{h,0}$, which is not singular anymore. Therefore, we can define the interface operator (Schur complement) $\widetilde{C}^0_\Sigma = C_{\Sigma\Sigma} - C_{\Sigma f}(C^0_{ff})^{-1}C_{f\Sigma}$.

Let $\mathbf{U}_d$ be the array of (assigned) velocity nodal values on the boundary $\partial\Omega_f \setminus \Sigma$. We use the subscript d for vectors and matrices associated to boundary nodes. Moreover, if $\mathbf{U}_f$ denotes the velocity degrees of freedom (on interior nodes only), the Dirichlet fluid sub-problem consists of: find $\mathbf{U}_f$ and $\mathbf{P}$ such that

$$\begin{bmatrix} A_{ff} & G_f \\ D_f & 0 \end{bmatrix} \begin{bmatrix} \mathbf{U}_f \\ \mathbf{P} \end{bmatrix} = \begin{bmatrix} \mathbf{b}_f \\ \mathbf{0} \end{bmatrix} - \begin{bmatrix} A_{fd}\mathbf{U}_d + A_{f\Sigma}\mathbf{U}_\Sigma \\ D_d\mathbf{U}_d + D_\Sigma\mathbf{U}_\Sigma \end{bmatrix}, \tag{25}$$

where $\begin{bmatrix} A_{ff} & G_f \\ D_f & 0 \end{bmatrix} = C_{ff}$. Then, the projected fluid sub-problem will be equivalent to the original one only if the right hand side $\mathbf{b}$ of (25) satisfies the solvability condition

$$\mathrm{proj}_{\mathrm{Ker}(C^T_{ff})}(\mathbf{b}) = 0, \tag{26}$$

that is

$$\mathbf{1}^T \cdot (D_d\mathbf{U}_d + D_\Sigma\mathbf{U}_\Sigma) = 0.$$

Denoting by ψ_i and $\boldsymbol{\phi}_i$ the pressure and velocity basis functions, if j is related to a node on the interface Σ, we have

$$\begin{aligned} \mathbf{1}^T \cdot D_\Sigma\mathbf{U}_\Sigma &= \sum_i \sum_j \int_{\Omega_f} \psi_i \nabla\cdot\boldsymbol{\phi}_j u_j \\ &= -\sum_i \sum_j \int_{\Omega_f} \nabla\psi_i \boldsymbol{\phi}_j u_j + \sum_i \sum_j \int_\Sigma \psi_i \boldsymbol{\phi}_j \cdot \boldsymbol{n}_f u_j \\ &= -\sum_j \int_{\Omega_f} \left(\sum_i \nabla\psi_i\right)\boldsymbol{\phi}_j, u_j + \sum_j \int_\Sigma \left(\sum_i \psi_i\right)\boldsymbol{\phi}_j \cdot \boldsymbol{n}_f\, u_j \\ &= \int_\Sigma \sum_j \boldsymbol{\phi}_j \cdot \boldsymbol{n}_f\, u_j, \end{aligned}$$

where the last equality comes to the partition of unity satisfied by the basis functions ψ_i. An analogous term comes from $\mathbf{1}^T \cdot D_d\mathbf{U}_d$. Therefore, the solvability condition (26) can be equivalently written as

$$\mathbf{h}^T \cdot \mathbf{U}_\Sigma = -g, \tag{27}$$

where

$$(\mathbf{h})_j = \int_\Sigma \boldsymbol{\phi}_j \cdot \boldsymbol{n}_f,$$

j being a node on the interface and

$$g = \int_{\Omega_f \setminus \Sigma} u_d.$$

Eq. (27) can be seen as a constraint on the interface velocity. Let us force this constraint through the introduction of a Lagrange multiplier λ (see [25]). We are led, therefore, to the "augmented" interface problem

$$\begin{bmatrix} \widetilde{N}_\Sigma + \widetilde{C}^0_\Sigma & \mathbf{h} \\ \mathbf{h}^T & 0 \end{bmatrix} \begin{bmatrix} \mathbf{U}_\Sigma \\ \lambda \end{bmatrix} = \begin{bmatrix} \tilde{\mathbf{b}}_\Sigma \\ -g \end{bmatrix}. \tag{28}$$

Having defined an augmented interface problem one can now define the "augmented" DN preconditioner as

$$\begin{bmatrix} \widetilde{N}_\Sigma & \mathbf{h} \\ \mathbf{h}^T & 0 \end{bmatrix}.$$

When applied together with Richardson or GMRES iterations, this entails, in particular, the solution of a fully Dirichlet fluid sub-problem and a constrained structure problem at each iteration.

We point out however that the enforcement of the solvability condition on the structure sub-problem couples all the interface nodes, with the subsequent dramatic increase of the matrix band width. Furthermore, this approach leads to a saddle-point problem for the structure, loosing the typical semi-positive definiteness.

An alternative strategy to tackle balloon-type problems using the DN preconditioner consists in adding a pseudo-compressibility term. This has been proposed in [38] as a way to make the fluid problem non-singular and has been relaxed along the iterative process (pseudo-compressibility iterations). The idea is to introduce in the mass conservation equation of the fluid formulation a term

$$\frac{1}{\epsilon}(p_h^{k+1} - p_h^k, q_h),$$

where k is the iteration counter and ϵ a positive numerical parameter. Therefore, once convergence is reached, the compressibility vanishes and the incompressible solution is attained. With the new term, the fluid problem is not singular anymore.

For the solution of such a problem one can deal with nested loops. Unfortunately, this method is too expensive because involves as many FSI solvers (using DN) as pseudo-compressibility iterations are needed. The DN method is very expensive by itself, and this method multiplies the CPU cost of DN by the number of pseudo-compressibility iterations. In order to make the method slightly less expensive, one-loop algorithms dealing with coupling and pseudo-compressibility iterations have been designed in [38]. However, it cannot be straightforwardly used with GMRES iterations.

7.2. Robin transmission conditions

Finally, we propose the schemes based on Robin transmission conditions as effective tools for the solution of FSI problems where the fluid is entirely enclosed by Dirichlet boundary conditions at $\partial\Omega_f \setminus \Sigma^t$. Indeed, using the partitioned procedures suggested in [2] and the related preconditioners proposed in this work, balloon-type problems can be straightforwardly solved without any extra modification.

In particular, focusing on the sequential RR Algorithm 1 the use of a Robin transmission condition for the fluid problem guarantees that the fluid matrix is invertible and the problem solvable no matter what boundary conditions are enforced on $\partial\Omega_f \setminus \Sigma$. Hence, we do not need to enforce any solvability condition to the structure problem, nor projecting the fluid equation on the subspace of zero average pressures. Furthermore, by imposing a Robin (or Neumann) boundary condition at the interface for the structure problem, it is also possible to deal with fully submerged incompressible structures.

A RR preconditioner to the interface problem (28) can be written as

$$P_{\mathrm{RR}} = \begin{bmatrix} \widetilde{C}^0_\Sigma + \alpha_f M_\Sigma & \boldsymbol{h} \\ \boldsymbol{h}^T & 0 \end{bmatrix} \begin{bmatrix} \frac{1}{\alpha_f+\alpha_s} M^{-1}_\Sigma & 0 \\ 0 & 1 \end{bmatrix} \begin{bmatrix} \widetilde{N}_\Sigma + \alpha_s M_\Sigma & 0 \\ 0 & 1 \end{bmatrix}.$$

Observe that the solution of a fluid problem with matrix $F_\Sigma = \begin{bmatrix} \widetilde{C}_\Sigma^0 + \alpha_f M_\Sigma & \boldsymbol{h} \\ \boldsymbol{h}^T & 0 \end{bmatrix}$ corresponds to a fluid problem with Robin boundary conditions at the interface, with no special modifications. Indeed, the Lagrange multiplier (mean pressure) can be added to the zero average pressure degrees of freedom to recover the original pressure space and, in fact, the matrix F_Σ coincides with the matrix $(\widetilde{C}_\Sigma + \alpha_f M_\Sigma)$ considered in (9).

Following the same arguments as in Lemmas 1 and 2 it can be shown that, also in case of an enclosed fluid problem, the RR-preconditioned Richardson algorithm leads to exactly the same sequence of solves described in Algorithm 1 whereas the RR-preconditioned GMRES algorithm leads to the same sequence of solves described in Algorithm 2. Therefore, these algorithms can be applied with no modification to encolsed flow problems.

As shown in [2], algorithms based on Robin transmission conditions are superior to DN in terms of efficiency, especially for high added-mass effect. For balloon-type problems, where modified (and even more expensive) versions of DN are needed, the use of RR methods are even more justified.

Remark 3. The same pathological case arising when DN preconditioners are applied to FSI problems with Dirichlet conditions over $\partial\Omega_f \setminus \Sigma$, occurs when flow rate boundary conditions

$$\int_{\partial\Omega_f \setminus \Sigma} \boldsymbol{u} \cdot \boldsymbol{n}_f \, d\gamma = Q$$

for a given scalar Q, are prescribed (see [17]). Also in this case RR methods can be applied with no modifications.

8. Numerical experimentation

In this section, we carry out some numerical tests in order to show the performances of the RN-GMRES algorithm with respect to RN-Richardson, DN-Richardson and DN-GMRES algorithms for problems with large added-mass effect and balloon-type problems. In all cases, multifrontal solvers have been used for fluid and structure sub-problems.

For both problems we choose a conforming space discretization between fluid and structure: stabilized $\mathbb{P}_1 - \mathbb{P}_1$ finite elements for the fluid, where the stabilization is the orthogonal subgrid scales approach (see e.g. [10]), and $\mathbb{P}_1$ finite elements for the structure. In all tests, the structural problem is a d-dimensional (where d is the space dimension) linear elastic solid. We refer to [4] for a detailed exposition of the formulation of the structural problem and to Table 2 for the parameters used for the fluid and structure problems.

The software that has been used is ZEPHYR, a multi-physics finite element code written in Fortran and developed at CIMNE-UPC (Barcelona). For the solution of the linear systems we have used SPARSKIT, developed by Yousef Saad (see [39]).

In particular, in Section 8.1.1 we analyze the sensitivity of RN-GMRES and RN-Richardson with respect to the value α_f and the performances of RN-GMRES and DN-GMRES algorithms for a wide range of structure densities in two-dimensional problems. In Sections 8.1.2 and 8.1.3, we show the effectiveness of RN-GMRES for three-dimensional problems. Finally, in Section 8.2 we show the numerical results obtained for a balloon-type problem consisting of a 3d cavity with one elastic wall and one inlet wall with prescribed flux. The remaining walls are rigid.

8.1. Hemodynamics applications with large added-mass effect

Three different problems with a large added-mass effect have been considered:

- A fully 3d problem, whose fluid domain is a cylinder of radius $R_0 = 0.5$ cm and length $L = 6$ cm;
- Its 2d approximation, obtained by intersecting the pipe with a plane;
- A carotid bifurcation using a realistic geometry.

Our goal is to simulate the propagation of a pressure pulse in an artery with deformable boundaries as the structure density varies. The fluid and structure physical parameters used in the simulations are the same as the ones employed in the analysis of Section 6.1 (see Table 2). However, the listed wall thickness does not apply for the carotid bifurcation test.

On the inflow section we impose the following Neumann boundary condition:

$$\boldsymbol{T}_f \cdot \boldsymbol{n}_f = \begin{cases} \frac{P_{in}}{2}\left[1 - \cos\left(\frac{\pi t}{2.5\times 10^{-3}}\right)\right]\boldsymbol{n}_f, & t < 5\times 10^{-3}, \\ \boldsymbol{0} & t \geqslant 5\times 10^{-3}, \end{cases}$$

while on the outflow section an homogeneous Neumann condition has been imposed. The amplitude P_{in} of the pressure pulse has been taken equal to 2×10^4 dyne/cm^2 and the time duration of the pulse is 5 ms. We solve the problem over the time interval [0, 0.012] s. Otherwise indicated, the time step size is $\Delta t = 4\times 10^{-4}$ s.

8.1.1. A 2d straight artery

We start by solving a classical benchmark in FSI interaction (see e.g. [29]). We consider a mesh with 1823 finite elements. In all cases, the stopping criterion is based on the relative difference between the interface velocity at two subsequent iterations

$$E_U^k := \frac{\|\mathbf{U}_\Sigma^{k+1} - \mathbf{U}_\Sigma^k\|}{\|\mathbf{U}_\Sigma^k\|},$$

which is known to be a good estimate of the relative error if the error reduction factor

$$\sigma := \lim_{k\to\infty} \sigma^k, \quad \sigma^k := \frac{\|\mathbf{U}_\Sigma - \mathbf{U}_\Sigma^{k+1}\|}{\|\mathbf{U}_\Sigma - \mathbf{U}_\Sigma^k\|} \tag{29}$$

is sufficiently small. Indeed, we have

$$\|\mathbf{U}_\Sigma - \mathbf{U}_\Sigma^k\| \leqslant \frac{1}{1-\sigma^k}\|\mathbf{U}_\Sigma^{k+1} - \mathbf{U}_\Sigma^k\|. \tag{30}$$

In particular, we require that $\|E_U^k\| < \varepsilon$, where the tolerance ε has been set equal to 10^{-6}.

A good value of the parameter α_f in the interface Robin condition for the fluid sub-problem can be obtained from the structure simplified model proposed in [30] and is given by

$$\alpha_f^{\text{opt}} = \frac{\rho_s H_s}{\Delta t} + \frac{\Delta t H_s E}{1-\nu^2}(4\rho_1^2 - 2(1-\nu)\rho_2), \tag{31}$$

where ρ_1 and ρ_2 are the mean and the Gaussian curvature of the interface, respectively. In this case, α_f^{opt} is a function of the position on the interface. In many realistic geometries the values of the curvatures are not easily available or even not computable directly (as in a geometry with edges). It is therefore reasonable, in these situations, to use an approximate value (even constant in space) for α_f (see Section 8.1.3). We are then interested in testing the robustness of the RR-based schemes with respect to the parameter α_f. To this aim, as first test we consider the RN-based schemes and a rectangular computational domain, for which a good value of α_f is known and given by (17) (see [30,2]). Using the values of Table 2, we have $\alpha_f^{\text{opt}} = 743.4$. In particular, this test consists of comparing the performance of RN-GMRES and RN-Richardson (with no relaxation) for different values of α_f. We consider $\alpha_f = \gamma\alpha_f^{\text{opt}}$ with different values of γ. The nonlinearities given by the domain position and by the convective term are treated in a semi-implicit way. The mean

number of iterations per time step and, in parentheses, the computational cost normalized to the cost of RN-GMRES with $\gamma = 1$ are summarized in Table 3.

As expected, RN-GMRES has the minimum number of iterations for $\gamma = 1$ (optimal value of α_f). The number of iterations increases when we take α_f smaller or larger than the optimal value. In any case, the increase is much more important for smaller values of α_f. These results show that RN-Richardson is much more sensitive to α_f. For the optimal value, the performance is similar to the one of RN-GMRES, as proved by the computational costs. Taking a tenth of the optimal α_f the convergence is so slow that we reach the maximum number of iterations without reaching tolerance.

In Fig. 5 we show the relative difference between the interface velocity at two subsequent iterations E_U^k along the iterative process at a given time step. The RN-Richardson method seems to converge (even though extremely slowly) to the solution, as we can see in Fig. 5b. However, for α_f much larger than the optimal value (ten times or more), the RN-Richardson does not converge (indeed, its behavior tends to the one of DN-Richardson which does not converge without any relaxation).

From this first test, we conclude that RN-GMRES is moderately sensitive to the choice of α_f, but much less than RN-Richardson. For this reason, the RN-Richardson algorithm is very useful when a sharp evaluation of α_f is available, but it does not work if we cannot get a good expression for α_f. On the contrary, the RN-GMRES scheme, thanks to its robustness, can be used with good performances also for those geometries for which an optimal value of α_f cannot be evaluated with precision, such as in the enclosed-domain simulation shown in Section 8.2.

The second test consists in evaluating the sensitivity of both RN-GMRES and DN-GMRES to the added-mass effect. A semi-implicit treatment of convective and domain nonlinearities is adopted. We have solved the 2*d* straight artery with the following values of the structure density:

$$\rho_s = 1, 10, 100, 1000\ \mathrm{g/cm^3}.$$

Table 3
2*d* Straight artery: average number of iterations and normalized CPU cost for RN-GMRES and RN-Richardson for different values of $\gamma(\alpha_f = \gamma\alpha_f^{\mathrm{opt}})$.

γ	RN-GMRES	RN-Richardson
0.01	21.53 (3.43)	>max. it.
0.1	15.47 (2.58)	>max. it.
1.0	5.07 (1.00)	8.933 (1.02)
10.0	10.13 (1.79)	No conv.
100.0	10.80 (1.83)	No conv.

For RN-GMRES, we have used the optimal value of α_f in (17). The results are listed in Table 4. RN-GMRES is extremely insensitive to the added-mass effect. On the contrary, as proved in [3], DN-GMRES is fairly sensitive to the added-mass effect. The number of fluid elements is 3.7 times larger than the structure elements. Therefore, the additional computational cost of the RN-GMRES iterations (one extra structural sub-problem) is not very important and the RN-GMRES algorithm is better than DN-GMRES both in number of iterations and CPU cost for large added-mass effect. From these results, we can state that RN-GMRES becomes more efficient than DN-GMRES as the added-mass effect increases and the CPU cost of the structure problem is small compared to the fluid one. These results are in good agreement with the previous theoretical analysis. In fact, the previous analysis says that the RN-GMRES reduction factor remains far from 1 as ρ_s is reduced whereas the DN-GMRES reduction factor tends to 1 (see Fig. 3a).

We finally consider one test comparing RN-GMRES and RN-Richardson for implicit treatment of the nonlinearities. For RN-Richardson, it is very easy to treat coupling iterations and nonlinearities using the same loop (one-loop algorithm). Therefore, only one tolerance is needed, simplifying the implementation. For RN-GMRES, we consider instead nested loops: an external loop for nonlinearities and an internal loop (GMRES iterations) for the FSI coupling. In this case, two tolerances are required. The nonlinear tolerance is set to 10^{-3}. The performance of the algorithm is highly dependent on an appropriate choice of the internal tolerance. In Table 5 we show that a very tight tolerance for the internal GMRES iterations leads to a very poor performance. The internal GMRES tolerance is so small that it requires lots of iterations, for every nonlinear iteration, that in fact are not needed. Using a much looser tolerance, the method "tends to a one-loop algorithm". In this case, the GMRES iterations easily converge and the tolerance that dictates the convergence is the external one. In any case, we can state that the one-loop RN-Richardson algorithm performs better than RN-GMRES for implicit treatment of the nonlinearities.

8.1.2. A 3d straight artery

The second problem we solve is the 3*d* straight artery, in order to show that the behavior that we have observed for a 2*d* problem also applies in the 3*d* case. We consider a semi-implicit scheme. Two different values of the coupling tolerance have been considered, 10^{-3} and 10^{-6}. When the tolerance is not reported, it has been set to 10^{-3}. Otherwise indicated, the time step size is $\Delta t = 10^{-4}$. The finite element mesh used for the computations has 21,575 finite elements.

The sensitivity of RN-GMRES and RN-Richardson algorithms with respect to the value of α_f is shown in Table 6 and Fig. 6.

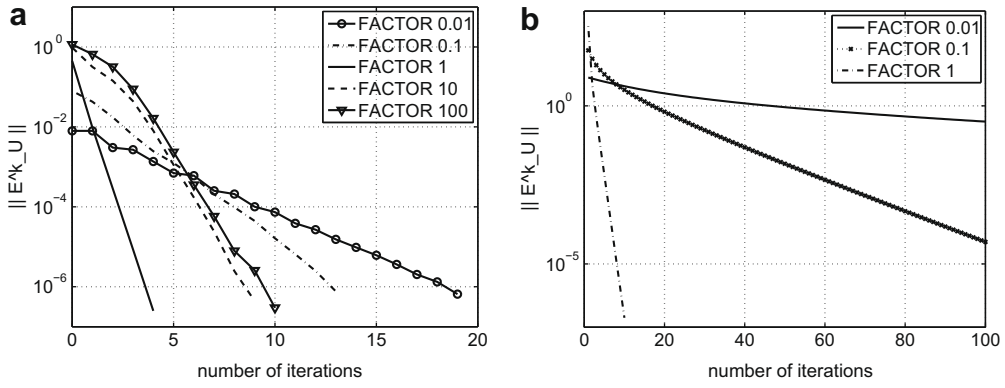

Fig. 5. 2*d* Straight artery: norm of E_U^k vs. iteration number for (a) RN-GMRES and (b) RN-Richardson with different values of α_f.

Table 4
2*d* Straight artery: average number of iterations and CPU cost normalized to the cost of RN-GMRES - $\rho_s = 1$, for RN-GMRES and DN-GMRES for different values of ρ_s.

ρ_s	RN-GMRES	DN-GMRES
1	5.20 (1.00)	11.73 (1.92)
10	6.00 (1.12)	7.87 (0.99)
100	4.73 (0.92)	5.93 (0.79)
1000	4.60 (0.90)	4.80 (0.66)

Table 5
2*d* Straight artery: average of accumulated RN-GMRES iterations for two different values of the GMRES tolerance vs. average of accumulated RN-Richardson iterations (one-loop algorithm).

Internal tol.	RN-GMRES	RN-Richardson
(One-loop)	6	93
10^{-1}	7.87	
10^{-6}	24.20	

Table 6
3*d* Straight artery: average number of iterations and CPU cost normalized to the cost of RN-GMRES - $\gamma = 1$, for RN-GMRES and RN-Richardson for different values of $\gamma(\alpha_f = \gamma\alpha_f^{\text{opt}})$. The first table corresponds to a tolerance of 10^{-3} and the second one to 10^{-6}.

γ	RN-GMRES (10^{-3})	RN-Richardson (10^{-3})
0.1	9.13 (2.01)	>max. it.
1.0	4.00 (1.00)	6.67 (0.98)
10.0	5.73 (1.34)	No conv.
	RN-GMRES (10^{-6})	RN-Richardson (10^{-6})
0.1	16.20 (1.60)	>max. it.
1.0	6.60 (1.00)	10.00 (1.41)
10.0	9.40 (0.54)	No conv.

The behavior is very similar to the one observed in the 2*d* case. RN-GMRES is less sensitive to α_f than in the 2*d* case. RN-Richardson is efficient for the optimal value of α_f but again has a very slow convergence or does not converge for bad choices of this parameter.

The sensitivity of RN-GMRES and DN-GMRES algorithms with respect to the added-mass effect is shown in Table 7. Again, RN-GMRES requires less iterations to reach convergence. This improvement is more evident increasing the added-mass effect. The number of iterations is a fair comparison of both methods in FSI applications where the structural problem is much cheaper than the fluid one. This is the situation in most real applications of interest. However, when the CPU cost related to the structural problem is an important part of the overall CPU cost, one RN-GMRES iteration (that involves an additional structure problem) becomes more expensive than one DN-GMRES iteration. We have considered a problem with 2.14 fluid elements per structure element. Moreover, we have listed in Table 7 the CPU cost normalized to the cost of RN-GMRES with $\rho_s = 1$ (in parentheses). The improvement of RN-GMRES over DN-GMRES is reduced as the structure problem CPU cost increases with respect to the fluid one.

Table 7
3*d* Straight artery: average number of iterations and normalized CPU cost for RN-GMRES and DN-GMRES for different values of ρ_s. The first value corresponds to a tolerance of 10^{-3} and the second one to 10^{-6}.

ρ_s	RN-GMRES (10^{-3})	DN-GMRES (10^{-3})
1	4.00 (1.00)	6.47 (1.04)
10	3.80 (0.96)	4.47 (0.75)
100	2.13 (0.63)	3.07 (0.56)
1000	2.53 (0.71)	3.00 (0.57)
	RN-GMRES (10^{-6})	DN-GMRES (10^{-6})
1	7.00 (1.00)	10.00 (0.95)
10	5.40 (0.81)	6.00 (0.61)
100	3.90 (0.62)	5.00 (0.52)
1000	3.90 (0.59)	4.00 (0.45)

Table 8
3*d* Straight artery: average number of iterations and CPU cost normalized to the cost of RN-GMRES – $\Delta t = 10^{-5}$, for RN-GMRES and DN-GMRES for different values of Δt. The values correspond to a tolerance of 10^{-6}.

Δt	RN-GMRES	DN-GMRES
10^{-5}	8.10 (1.00)	13.00 (1.28)
5×10^{-4}	7.25 (0.92)	10.05 (1.02)

In Table 8 we report a comparison of DN-GMRES and RN-GMRES methods for two different time step sizes. The RN-GMRES algorithm seems to be less sensitive to the time step size, whereas the number of DN-GMRES iterations clearly increases as the time step size decreases. In this case we have considered a tolerance of 10^{-6} for the GMRES loop. Therefore, the RN-GMRES algorithm also becomes more effective than DN-GMRES as the time step size is reduced.

8.1.3. The carotid bifurcation

Finally, we employ the RN-GMRES on a real geometry of a human carotid, in physiological conditions. The finite element mesh consists of 42,304 finite elements. In Fig. 7, the pressure wave traveling along the carotid is shown at 4 different instants.

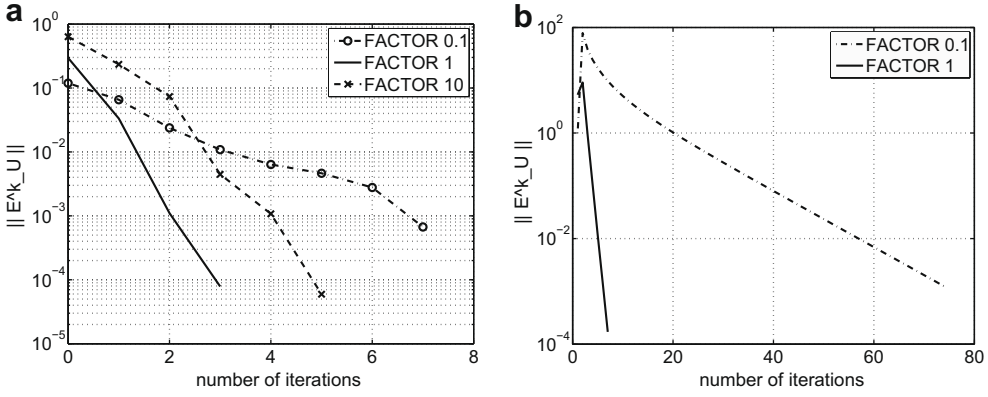

Fig. 6. 3*d* Straight artery: norm of E_U^k vs. iteration number for (a) RN-GMRES and (b) RN-Richardson with different values of α_f.

As observed from expression (31), in this case the optimal value based on a simplified structural model for α_f is not constant. However, in this example we take a simplified approach and construct a constant α_f using expression (17) where an average value of the radius (0.33 cm) and thickness (0.08 cm) of the carotid are used. The use of non-constant α_f depending on the curvature will be investigated in a future work.

Due to the fact that the value of α_f is not so good as for the previous examples, the behavior of RN-Richardson, as expected, is much worse than the one of RN-GMRES, which is much less sensitive to α_f (see Fig. 8b). Moreover, the error reduction factor (29) can be approximated by the quantity

$$\sigma^k \simeq \frac{\|\mathbf{U}_\Sigma^{k+1} - \mathbf{U}_\Sigma^k\|}{\|\mathbf{U}_\Sigma^k - \mathbf{U}_\Sigma^{k-1}\|}.$$

Referring to the carotid bifurcation simulation, we estimate $\sigma^k \simeq 0.18$ for RN-GMRES and $\sigma^k \simeq 0.36$ for DN-GMRES (see Fig. 8a). Therefore, despite the non-optimal value of α_f, RN-GMRES seems to be superior to DN-GMRES in terms of convergence rate. Moreover, in both cases the approximated error reduction factor is sufficiently small to consider E_U^k as a good estimate of the relative error (see (30)). In Table 9, we show the average number of iterations for these two algorithms, with different values of α_f for RN-GMRES. The sensitivity of RN-GMRES with respect to α_f is

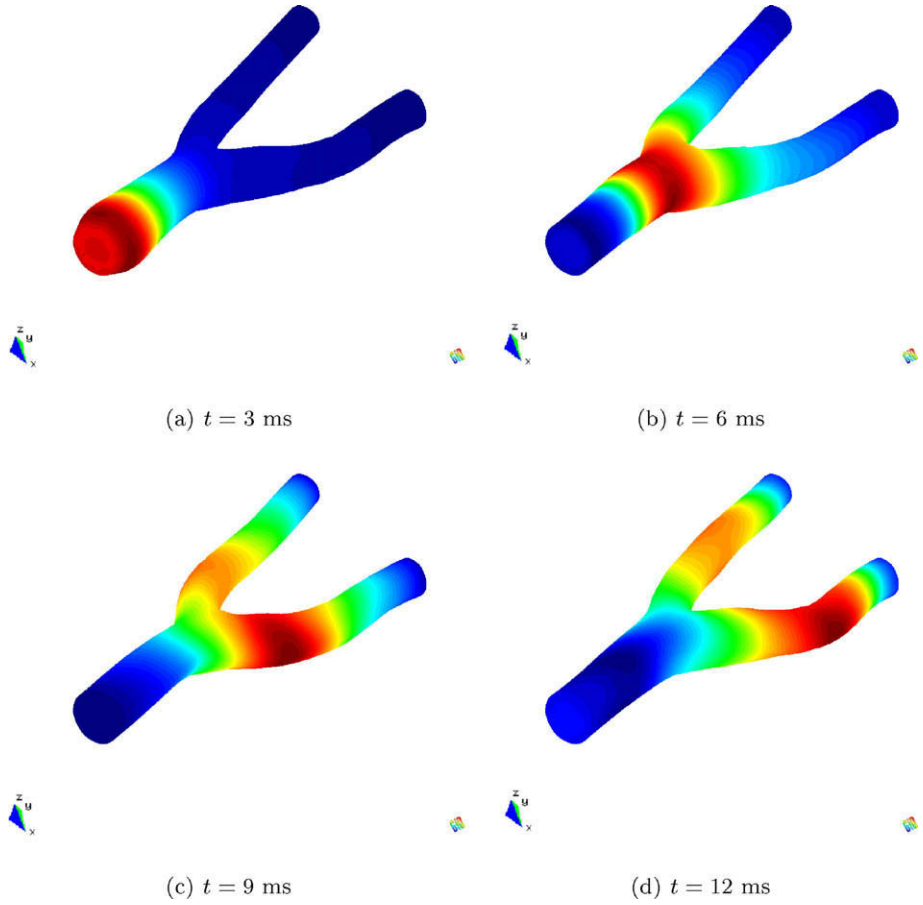

Fig. 7. Propagation of the initial pressure pulse in the carotid geometry, moving from the inflow to the outflow section. Solution at every 3 ms.

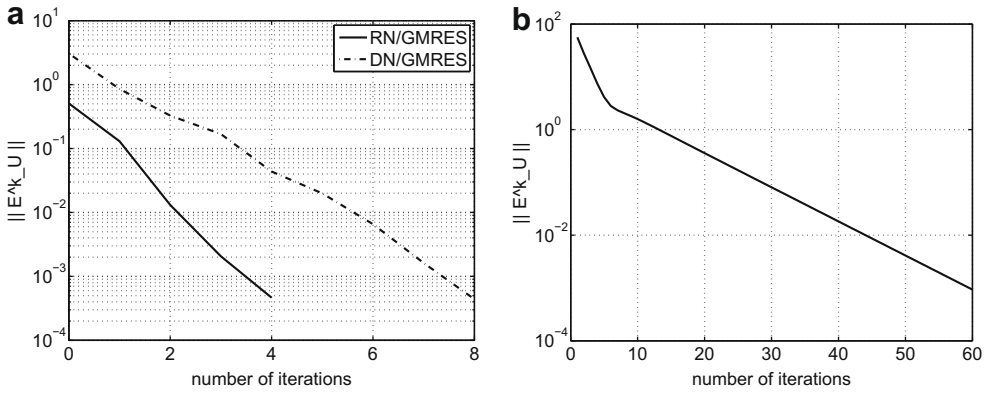

Fig. 8. Carotid bifurcation: norm of E_U^k vs. iteration number for (a) RN-GMRES with α_f^{opt} and DN-GMRES; (b) RN-Richardson with α_f^{opt}.

similar to what we have observed from the previous tests. The RN-GMRES algorithm with the optimal choice of α_f reduces the CPU cost (in Table 9 normalized to the cost of RN-GMRES - $\gamma = 1$) even for 1.95 fluid elements per structure element. In applications where the ratio between the number of structure elements and fluid elements is smaller, this saving in CPU time should increase.

8.2. Enclosed domains: a balloon-type problem

With respect to balloon-type problems, we have solved a 3*d* cavity with one elastic wall, in which we have enforced the inflow velocity. We have simulated the inflation and deflation processes.

Table 9
Carotid bifurcation: average number of iterations and normalized CPU cost for RN-GMRES and DN-GMRES for different values of $\alpha_f = \gamma \alpha_f^{\text{opt}}$.

γ	RN-GMRES	DN-GMRES
0.1	7.80 (1.32)	
1.0	5.13 (1.00)	8.80 (1.10)
10.0	8.33 (1.40)	

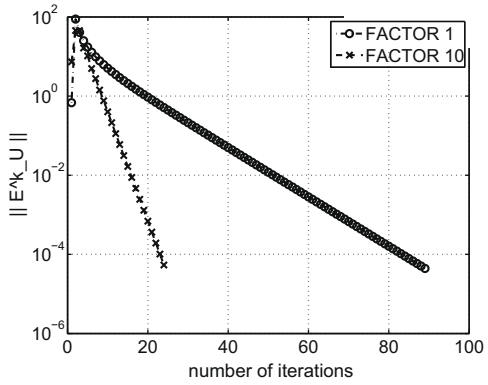

Fig. 9. Balloon problem: norm of E_U^k vs. iteration number for RN-Richardson with two values of α_f.

Table 10
Balloon problem: average number of iterations for RN-GMRES and two different values of γ and Δt.

	$\Delta t = 10^{-3}$	$\Delta t = 5 \times 10^{-3}$
$\gamma = 1$	6.32	8.68
$\gamma = 10$	4.02	3.81

In particular, we consider a problem similar to the one in [38]: the fluid domain Ω_f is the unit cube $[0,1] \times [0,1] \times [0,1]$ cm. The domain has been partitioned into 14,851 finite elements. The side on the plane $x = 0$ is where we enforce the inflow Dirichlet boundary condition

$$\boldsymbol{u}(\boldsymbol{x}, t) = f(t)\boldsymbol{v}(\boldsymbol{x}),$$

where $\boldsymbol{v}(\boldsymbol{x})$ is the parabolic profile

$$v_x = 16(y^2 - y)(z^2 - z),$$
$$v_y = 0,$$
$$v_z = 0,$$

and $f(t) = \sin\left(\frac{\pi t}{0.04}\right)$ defines the time evolution. The side on the plane $x = 1$ is the fluid–structure interface Σ. The structure is a wall of thickness 0.1 cm. On the remaining sides of $\partial\Omega_f$, no-slip boundary conditions are imposed. As we can see from the inflow boundary conditions, at $t = 0.08$ we must recover the initial volume of 1 cm^3. On the other hand, at $t = 0.04$ the maximum volume is attained. In the numerical experiments the tolerance in the FSI iterations is 10^{-4} and the time step size is 10^{-3} (if not otherwise indicated). The nonlinearities are treated in a semi-implicit way.

The same properties in Table 2 have been used in this case, as well as similar spatial dimensions. Therefore, this problem is in the range of hemodynamics applications.

In this case it is not so easy to get a good constant estimate for α_f and then we have considered the following choice:

$$\alpha_f = \frac{\gamma \rho_s H_s}{\Delta t}, \tag{32}$$

where $\gamma > 0$, i.e. α_f is obtained from (31) by dropping the terms including the curvatures and weighting the remaining "inertial" term with a suitable coefficient γ. An improved expression of α_f could be obtained by evaluating the curvature of the structure (see [30]). First, we have solved the problem using RN-Richardson. As commented above, this approach is very sensitive to α_f, and requires a very good expression of this value in order to be effective. In this case, where α_f only involves inertia terms, its behavior is not good. We show the reduction of the interface residual for RN-Richardson in Fig. 9, using (32) with $\gamma = 1$ and 10. The method performs better for the larger value of α_f, but it does not converge for $\gamma = 100$. On the other hand, we have solved the problem using the more robust RN-GMRES algorithm. In Table 10 we show the average number of iterations for the same values of γ used for RN-Richardson and two different time step sizes. The method exhibits a better behavior for $\gamma = 10$ although the convergence is attained in a fairly low number of iterations in both cases. From the expression (32), we can see that the value of α^f increases as the time step size decreases and therefore the importance of the inertia term with

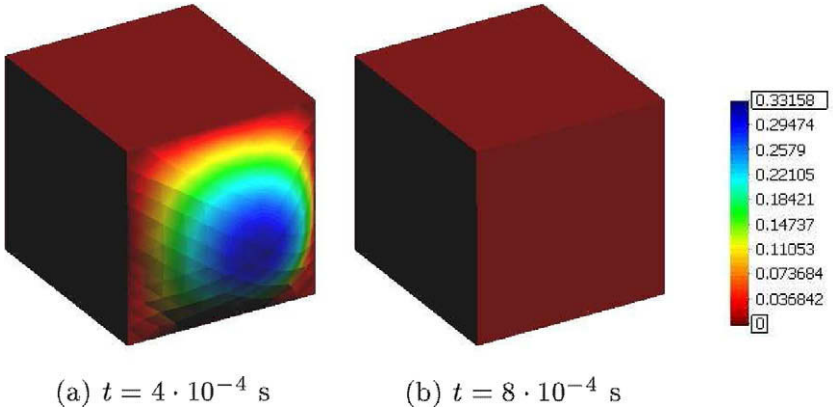

(a) $t = 4 \cdot 10^{-4}$ s (b) $t = 8 \cdot 10^{-4}$ s

Fig. 10. Balloon problem: deformed configuration of the balloon problem and contour fill of displacements at two different instants.

respect to other structural terms increases. For this reason, for a smaller time step size, the improvement of using $\gamma = 10$ instead of 1 is not so clear as for the large time step size. In any case, for both methods the choice of $\gamma = 10$ is clearly the best one.

Fig. 10a shows the deformed configuration and the displacement (in modulus) at time $t = 0.04$ s, when the maximum volume is attained. Fig. 10b shows the same at $t = 0.08$ s, where the initial configuration has been recovered without loss of volume.

In conclusion, we can state that the RN-GMRES is able to solve this balloon-type problem without any modification in the scheme (such as the introduction of a Lagrange multiplier or a pseudo-compressibility term) with physical and numerical properties in the range of hemodynamics applications (which implies a large added-mass effect) in a fairly low number of iterations. Let us remind that a direct application of the DN preconditioner is unfeasible.

9. Conclusions

In this article, we have reinterpreted the Robin–Robin (RR) partitioned procedure proposed in [2] as preconditioned iterations over the interface FSI problem. This has allowed us to define an interface RR preconditioner and apply it together with GMRES iterations, leading to the so-called RR-GMRES algorithm. Two different RR preconditioners have been designed, a parallel and a sequential one. The sequential preconditioner performs much better than the parallel one. Therefore, only the former has been extensively analyzed.

The convergence of the RN-GMRES algorithm has been analyzed on a simplified blood-vessel system. We have obtained the expression of the reduction factor and we have analyzed its sensitivity with respect to some important parameters. In particular, a comparison of the reduction factor of RN-GMRES and DN-GMRES (the latter found in [3]) leads to the following conclusions:

- The RN-GMRES always guarantees better performances, in particular in the range of parameters which leads to a high added-mass effect and for small time steps, situations where the DN-based schemes is known to be characterized by a slow convergence (see [3]).
- A good coefficient for the Robin transmission condition on the structure problem may be hard to find. Even reasonable choices of α_s (which however are difficult to generalize to complex problems) leads to performances of the RR strategy poorer than the RN one.

Numerical tests confirm the behavior foreseen by the theoretical investigation and to draw further conclusions:

- The new RN-GMRES algorithm becomes superior to the DN-GMRES algorithm as the added-mass effect increases or the time step size is reduced and the CPU cost of solving the structure sub-problem is small compared to the one of the fluid.
- RN-GMRES is more robust with respect to some geometrical and physical parameters than RN-Richardson. In particular, it is shown to be less sensitive to the parameter α_f used in the interface Robin condition for the fluid sub-problem. This has a very practical consequence, since it suggests to use RN-GMRES instead of RN-Richardson in those situations where the curvatures of the FS interface are not available or difficult to compute.
- RN-Richardson is still competitive for an implicit treatment of the nonlinearity when a very effective Robin transmission condition can be motivated. This is due to the fact that we can adopt a one loop strategy dealing with interface coupling and nonlinear iterations at the same time. On the contrary, Using GMRES, there is not a straight way to merge these two iterative processes, but the CPU cost can be clearly reduced using a loose tolerance for the inner (coupling) loop.
- Balloon-type problems cannot be solved with the classical DN preconditioner. Modified DN algorithms specifically designed for this kind of problems reduce the modularity (straight use of pre-existing fluid and structure solvers without internal modification) and increase the computation cost. RR (or RN)-based algorithms applied to this kind of problems are very effective and do not need any modification in the fluid and/or structure codes.Again, RN-GMRES performs much better than RN-Richardson when a sharp estimate of α_f is not available.

All these considerations allow us to state that the RN-GMRES algorithm is the most robust and most efficient modular approach for the solution of hemodynamics applications (or similar situations) and balloon-type problems among the methodologies considered in this work.

References

[1] A. Alonso, L. Trotta, A. Valli, Coercive domain decomposition algorithms for advection–diffusion equations and systems, J. Comput. Appl. Math. 96 (1998) 51–76.

[2] S. Badia, F. Nobile, C. Vergara, Fluid–structure partitioned procedures based on Robin transmission conditions, J. Comput. Phys. 227 (2008) 7027–7051.

[3] S. Badia, A. Quaini, A. Quarteroni, Modular vs. non-modular preconditioners for fluid–structure systems with large added-mass effect, Comput. Methods Appl. Mech. Engrg. 197 (2008) 4216–4232.

[4] S. Badia, A. Quaini, A. Quarteroni, Splitting methods based on algebraic factorization for fluid–structure interaction, SIAM J. Sci. Comput. 30 (4) (2008) 1778–1805.

[5] S. Badia, A. Quaini, A. Quarteroni, Coupling Biot and Navier–Stokes equations for modelling fluid–poroelastic media interaction, UPCommons, submitted for publication, <http://hdl.handle.net/2117/2549>.

[6] Y. Bazilevs, V.M. Calo, T.J.R. Hughes, Y. Zhang, Isogeometric fluid–structure interaction: theory, algorithms, and computations, Comput. Mech. 43 (2008) 3–37.

[7] Y. Bazilevs, V.M. Calo, Y. Zhang, T.J.R. Hughes, Isogeometric fluid–structure interaction analysis with applications to arterial blood flow, Comput. Mech. 38 (2006) 310–322.

[8] E. Burman, M.A. Fernández, Stabilized explicit coupling for fluid–structure interaction using Nitsche's method, C.R. Acad. Sci. Paris Sér. I Math. 345 (2007) 467–472.

[9] P. Causin, J.F. Gerbeau, F. Nobile, Added-mass effect in the design of partitioned algorithms for fluid–structure problems, Comput. Methods Appl. Mech. Eng. 194 (42–44) (2005) 4506–4527.

[10] R. Codina, A stabilized finite element method for generalized stationary incompressible flows, Comput. Methods Appl. Mech. Engrg. 190 (2001) 2681–2706.

[11] S. Deparis, M. Discacciati, G. Fourestey, A. Quarteroni, Fluid–structure algorithms based on Steklov–Poincaré operators, Comput. Methods Appl. Mech. Engrg. 195 (41–43) (2006) 5797–5812.

[12] M. Discacciati, A. Quarteroni, A. Valli, Robin–Robin domain decomposition methods for the Stokes–Darcy coupling, SIAM J. Numer. Anal. 45 (3) (2007) 1246–1268.

[13] J. Donea, An arbitrary Lagrangian–Eulerian finite element method for transient dynamic fluid–structure interaction, Comput. Methods Appl. Mech. Engrg. 33 (1982) 689–723.

[14] M.A. Fernández, J.F. Gerbeau, C. Grandmont, A projection semi-implicit scheme for the coupling of an elastic structure with an incompressible fluid, Int. J. Numer. Methods Engrg. 69 (4) (2007) 794–821.

[15] M.A. Fernández, M. Moubachir, A Newton method using exact Jacobians for solving fluid–structure coupling, Comput. Struct. 83 (2–3) (2005) 127–142.

[16] C. Figueroa, I. Vignon-Clementel, K. Jansen, T. Hughes, C. Taylor, A coupled momentum method for modeling blood flow in three-dimensional deformable arteries, Comput. Methods Appl. Mech. Engrg. 195 (2006) 5685–5706.

[17] L. Formaggia, A. Veneziani, C. Vergara, Numerical solution of flow rate boundary problems for an incompressible fluid in deformable domains, MOX Report n. 6, <http://mox.polimi.it> >>Research>>Publications>>Reports.

[18] C. Forster, W. Wall, E. Ramm, Artificial added mass instabilities in sequential staggered coupling of nonlinear structures and incompressible viscous flow, Comput. Methods Appl. Mech. Engrg. 196 (7) (2007) 1278–1293.

[19] F. Gastaldi, L. Gastaldi, A. Quarteroni, Adaptive domain decomposition methods for advection dominated equations, East–West J. Numer. Math 4 (1996) 165–206.

[20] J.F. Gerbeau, M. Vidrascu, A quasi-Newton algorithm based on a reduced model for fluid–structure interaction problems in blood flows, Math. Model. Numer. Anal. 37 (4) (2003) 631–648.

[21] L. Gerardo Giorda, P. Le Tallec, F. Nataf, A Robin–Robin preconditioner for advection–diffusion equations with discontinuous coefficients, Comput. Methods Appl. Mech. Engrg. 193 (9–11) (2004) 745–764.
[22] C. Grandmont, Analyse Mathematique et Numerique de Quelques Problemes d Interaction Fluid–Structure. Ph.D. Thesis, Laboratoire d Analyse Numrique de Paris VI, 1998.
[23] M. Heil, An efficient solver for the fully coupled solution of large-displacement fluid–structure interaction problems, Comput. Methods Appl. Mech. Engrg. 193 (2004) 1–23.
[24] T.J.R. Hughes, W.K. Liu, T.K. Zimmermann, Lagrangian–Eulerian finite element formulation for incompressible viscous flows, Comput. Methods Appl. Mech. Engrg. 29 (3) (1981) 329–349.
[25] U. Küttler, C. Forster, W.A. Wall, A solution for the incompressibility dilemma in partitioned fluid–structure interaction with pure Dirichlet fluid domains, Comput. Mech. 38 (2006) 417–429.
[26] P.L. Lions. On the Schwartz alternating method iii, in: T. Chan, R. Glowinki, J. Periaux, O.B. Widlund, (Eds.), Proceedings of the Third International Symposium on Domain Decomposition Methods for PDE's, Siam, Philadelphia, 1990, pp. 202–223.
[27] C. Michler, E.H. van Brummelen, R. de Borst, An interface Newton–Krylov solver for fluid–structure interaction, Int. J. Numer. Methods Fluids 47 (10–11) (2005) 1189–1195.
[28] C. Michler, E.H. van Brummelen, R. de Borst, Error-amplification analysis of subiteration-preconditioned GMRES for fluid–structure interaction, Comput. Methods Appl. Mech. Engrg. 195 (2006) 2124–2148.
[29] F. Nobile, Numerical Approximation of Fluid–Structure Interaction Problems with Application to Haemodynamics, Ph.D. Thesis, École Polytechnique Fédérale de Lausanne, 2001, Thesis n° 2458.
[30] F. Nobile, C. Vergara, An effective fluid–structure interaction formulation for vascular dynamics by generalized Robin conditions, SIAM J. Sci. Comput. 30 (2) (2008) 731–763.
[31] J.B. Perot, An analysis of the fractional step method, J. Comput. Phys. 108 (1993) 51–58.
[32] S. Piperno, C. Farhat, Partitioned prodecures for the transient solution of coupled aeroelastic problems – Part II: Energy transfer analysis and three-dimensional applications, Comput. Methods Appl. Mech. Engrg. 190 (2001) 3147–3170.
[33] A. Quaini, A. Quarteroni, A semi-implicit approach for fluid–structure interaction based on an algebraic fractional step method, M3AS 17 (6) (2007) 957–983.
[34] A. Quarteroni, F. Saleri, A. Veneziani, Analysis of the Yosida method for the incompressible Navier–Stokes equations, J. Math. Pures Appl. 78 (1999) 473–503.
[35] A. Quarteroni, F. Saleri, A. Veneziani, Factorization methods for the numerical approximation of Navier–Stokes equations, Comput. Methods Appl. Mech. Engrg. 188 (2000) 505–526.
[36] A. Quarteroni, M. Tuveri, A. Veneziani, Computational vascular fluid dynamics: problems, models and methods, Comput. Visual. Sci. 2 (2000) 163–197.
[37] A. Quarteroni, A. Valli, Domain Decomposition Methods for Partial Differential Equations, Oxford Science Publications, 1999.
[38] P. Raback, J. Ruokolainen, M. Lyly, E. Jarvinen. Fluid–structure interaction boundary conditions by artificial compressibility, in: ECCOMAS Computational Fluid Dynamics Conference, Swansea, Wales, UK, 2001.
[39] Y. Saad, SPARSKIT: A Basic Tool for Sparse Matrix Computation, Technical Report CSRD TR 1029, CSRD, University of Illinois, 1990.
[40] Y. Saad, Iterative Methods for Sparse Linear Systems, PWS Publishing, Boston, MA, 1996.
[41] P. Le Tallec, J. Mouro, Fluid structure interaction with large structural displacements, Comput. Methods Appl. Mech. Engrg. 190 (2001) 3039–3067.
[42] T.E. Tezduyar, S. Sathe, T. Cragin, B. Nanna, B.S. Conklin, J. Pausewang, M. Schwaab, Modelling of fluid–structure interactions with the space-time finite elements: arterial fluid mechanics, Int. J. Numer. Methods Fluids 54 (2007) 901–922.
[43] T.E. Tezduyar, S. Sathe, M. Schwaab, B.S. Conklin, Arterial fluid-mechanics modeling with the stabilized space-time fluid–structure interaction technique, Int. J. Numer. Methods Fluids 57 (2008) 601–629.
[44] E.H. van Brummelen, Added mass effect of compressible and incompressible flows in fluid–structure interaction, J. Appl. Mech. 76 (2009) 021206.